The nanophthalmos protein TMEM98 inhibits MYRF self-cleavage and is required for eye size specification

Short title: *Tmem98* and eye size specification

Sally H. Cross[1*], Lisa Mckie[1], Toby W. Hurd[1], Sam Riley[1], Jimi Wills[1], Alun R. Barnard[2], Fiona Young[3], Robert E. MacLaren[2] and Ian J. Jackson[1,4]

[1]MRC Human Genetics Unit, MRC Institute of Genetics and Molecular Medicine, University of Edinburgh, Edinburgh, United Kingdom

[2]Nuffield Laboratory of Ophthalmology, Nuffield Department of Clinical Neurosciences, University of Oxford, The John Radcliffe Hospital, Oxford, United Kingdom

[3]Electron Microscopy, Pathology, Western General Hospital, Edinburgh, United Kingdom

[4]Roslin Institute, University of Edinburgh, Easter Bush, Midlothian, United Kingdom

* Corresponding author

E-mail: sally.cross@igmm.ed.ac.uk

Abstract

The precise control of eye size is essential for normal vision. *TMEM98* is a highly conserved and widely expressed gene which appears to be involved in eye size regulation. Mutations in human *TMEM98* are found in patients with nanophthalmos (very small eyes) and variants near the gene are associated in population studies with myopia and increased eye size. As complete loss of function mutations in mouse *Tmem98* result in perinatal lethality, we produced mice deficient for *Tmem98* in the retinal pigment epithelium (RPE), where *Tmem98* is highly expressed. These mice have greatly enlarged eyes that are very fragile with very thin retinas. To gain insight into the mechanism of action we used a proximity labelling approach to discover interacting proteins and identified MYRF as an interacting partner. Mutations of *MYRF* are also associated with nanophthalmos. The protein is an endoplasmic reticulum-tethered transcription factor which undergoes autoproteolytic cleavage to liberate the N-terminal part which then translocates to the nucleus where it acts as a transcription factor. We find that TMEM98 inhibits the self-cleavage of MYRF, in a novel regulatory mechanism. In RPE lacking TMEM98, MYRF is ectopically activated and abnormally localised to the nuclei.

Author summary

Having the correct eye size is important, too large and you will be short-sighted and too small and you will be far-sighted. Nanophthalmos, literally very small eye from the Greek, is a condition where the eye is very small but structurally normal. In addition to being farsighted such eyes are prone to glaucoma which can lead to loss of vision. Here we studied a protein called TMEM98 which is found in the

membranes of the cells which form a layer at the back of eye called the retinal pigment epithelium (RPE). Mutations in *TMEM98* have been found in nanophthalmos patients. Patients have one normal copy of the gene and one carrying a mutation. We removed *Tmem98* from the RPE of mice in order to ascertain its function. We found, surprisingly, that rather than having small eyes this led to the development of very large eyes that were structurally fragile. We went to on to identify protein partners of TMEM98 and found that it interacts with a protein called MYRF, mutations in which also causes nanophthalmos. This work demonstrates the importance of *TMEM98* in eye size specification.

Introduction

Myopia and hyperopia impose a considerable disease burden in human populations and the incidence of refractive errors of the eye, myopia in particular, has increased greatly in the past few decades [1]. A critical factor in the development of refractive error is eye size, in particular axial length; too long and the eye is myopic, too short and it is hyperopic. Accurate control of eye growth is thus essential for normal vision. Whilst changes in human behaviour and environmental factors have played a part in the world-wide increase in myopia, genetic specification of eye size is also important. Many genes have been identified that are implicated in the occurrence of refractive error and thus of eye size [2-5]. Among these is *TMEM98*, mutations of which have also been found to be associated with dominant nanophthalmos [6, 7]. Variants close to the 5' end of *TMEM98* are associated with myopia in genome wide association studies [2, 4, 5], in which the minor alleles are associated with myopia and most likely a larger eye.

TMEM98 encodes a highly conserved 226 amino acid transmembrane protein. It was initially reported to be part of an expression signature characteristic of adenocarcinoma, a subtype of adenosquamous carcinoma, a type of cervical cancer [8]. Subsequently it was suggested to be a novel chemoresistance-conferring gene in heptacellular carcinoma [9]. It has also been reported to be able to promote the differentiation of T helper 1 cells [10]. Studies using small interfering RNAs to knockdown expression of *TMEM98* have pointed to it having a role in the invasion and migration of lung cancer cells and in atherosclerosis [11, 12] and it may also be important for wound healing [13]. *TMEM98* was one of a set of genes used to construct a developmental hierarchy of breast cancer cells which could inform treatment strategies and disease prognosis [14].

However, two missense mutations in *TMEM98*, A193P and H196P, and a small deletion that removes the distal part of exon 4 and the beginning of the adjacent intron are associated with dominant nanophthalmos in humans [6, 7]. When we introduced the two human disease-associated missense mutations into the mouse gene we found no dominant phenotype [15]. However, when homozygous or as compound heterozygous these mutations caused a progressive retinal folding phenotype but we observed no significant change in eye size [15]. A different missense mutation in *Tmem98*, I135T, was found to cause a similar dominant retinal phenotype but was homozygous lethal [15]. The eyes of mice that are heterozygous for a knockout allele for *Tmem98* are normal showing that in the mouse haploinsufficiency for *Tmem98* does not cause an eye phenotype [15]. When pathogenic mutations in other genes causing nanophthalmos in humans have been studied in mice it has also been found that significant changes in eye size do not

result, rather the predominant phenotype is retinal defects in line with what we found with *Tmem98* [16-27].

The homozygous lethality of a global *Tmem98* knockout precluded the possibility of studying the adult eye phenotype. To address the question of the importance of *Tmem98* expression in eye development we have knocked-out *Tmem98* specifically in the eye and find that an enlarged eye results. Both the phenotype of human patients and the mouse knockout phenotype indicate the importance of *TMEM98* in eye size specification. We have gone on to examine the function of TMEM98 by identifying interacting proteins and find that it binds to, and prevents the self-cleavage, of the myelin regulatory factor, MYRF. The *MYRF* gene is itself associated with mutations leading to nanophthalmos [28-31] thus identifying a pathway critical for eye size specification.

Results

Knockout of *Tmem98* causes eye enlargement, retinal and RPE abnormalities

Tmem98 encodes a highly conserved 226 amino acid transmembrane protein. In the eye it is expressed during development in the RPE, and to a lesser extent in the ganglion cell layer (Fig 1A). In the adult eye it is expressed in the RPE, ciliary body and the iris (S1 Fig) [15].

As variants or mutations in human *TMEM98* are associated with larger or smaller eyes in humans we aimed to examine the role of the protein in eye development, and in particular the phenotype of a knockout of the gene in mice. First we examined the eyes of homozygous knockout mice at late stages of foetal

development. At embryonic day (E)16.5-E17.5 the eyes of the majority (5/6) knockout mice have an elongated shape when compared to wild-type and heterozygous knockout eyes (Fig 1B), suggesting that loss of *Tmem98* impacts control of eye size. As complete knockout of *Tmem98* is perinatal lethal [15] to examine the phenotype of adult eyes in the absence of *Tmem98* we generated mice where *Tmem98* is knocked-out only in the eye. We converted the "knockout-first" allele $Tmem98^{tm1a}$ to the conditional allele $Tmem98^{tm1c}$ as described in Materials and Methods. In the presence of Cre the floxed critical exon 4 in the $Tmem98^{tm1c}$ allele is removed, generating a deletion allele that has a frameshift, $Tmem98^{tm1d}$.The eyes of mice homozygous for the conditional allele, $Tmem98^{tm1c/tm1c}$ (S2 Fig) and compound heterozygotes for the conditional with the deletion allele, $Tmem98^{tm1c/tm1d}$ (Fig 2B, 2D, 3B) are normal. To knockout *Tmem98* in the RPE we used mice carrying the Tyr-Cre transgene, where Cre recombinase is expressed under the control of the tyrosinase promoter in the RPE and melanocytes derived from the neural crest [32, 33]. We verified where in the eye the Tyr-Cre transgene was expressed by examining mice that carried both the Tyr-Cre transgene and the R26MTMG transgene. The R26MTMG transgene expresses the tomato fluorescent protein ubiquitously under the control of the *Rosa26* promoter except in cells expressing Cre where the tomato is excised and green fluorescent protein is expressed instead [34]. This showed that the Tyr-Cre transgene is active in the RPE, ciliary body and iris (S3 Fig), all also sites of expression of *Tmem98* (Fig 1A and S1 Fig). By crossing $Tmem98^{tm1d/+}$; Tyr-Cre mice with $Tmem98^{tm1c/tm1c}$ mice we generated $Tmem98^{tm1c/tm1d}$; Tyr-Cre mice and control littermates. As expected, because *Tmem98* expression was only absent in the eye, these conditionally knocked-out mice were viable and fertile. Unexpectedly, given the association between *Tmem98*

and nanophthalmos, adult eyes in which *Tmem98* had been knocked-out by Tyr-Cre were greatly enlarged (Fig 2A-C) and fundal imaging revealed that there was extensive retinal degeneration in the mutant eyes (Fig 2D). These abnormalities were not observed in mice with Tyr-Cre and at least one functional copy of *Tmem98* indicating that Cre expression alone did not elicit any defects (Fig 2B, 2D).

To further investigate the retinal phenotype we examined mutant and control eyes by scanning laser ophthalmoscopy (SLO) (Fig 2E). Infrared (IR) reflectance and multicolour mode imaging confirmed the observation of retinal degeneration in mutant eyes shown in colour fundus photographs; compared to the largely homogenous background of wild-type eyes, mutant eyes had a more disrupted and granular appearance. Blue autofluorescence (BAF) imaging showed conditional mutant retinas to have a reduction in the overall background level of autofluorescence but with a higher number of hyperfluorescent puncta compared to wild-type eyes, further confirming retinal degeneration and suggesting unhealthy and/or loss of RPE cells. Imaging with the near infrared autofluorescence (IRAF) mode showed that the overall level of signal was reduced in mutant eyes compared to wild-types, such that recording a reliable averaged image was not possible in the former.

The RPE and retina are abnormal in the *Tmem98* conditional knockout

In RPE lacking *Tmem98* the cellular architecture is highly aberrant (Fig 3A). To study the morphology of the RPE we stained flat mount preparations of RPE for ZO1 (also known as TJP1) which is located at tight junctions between cells [35]. In the control, staining for ZO1 outlines the typical regular hexagonal shape of the RPE cells which

contain either one or two nuclei (Fig 3A, left). In contrast, the mutant RPE lacking *Tmem98* has a highly irregular pattern of polygonal-sided cells which vary greatly in both their size and the number of sides and many are multinucleated (Fig 3A, right). The presence of these large irregular cells may indicate that cell death has occurred and that the remaining cells have enlarged and fused to compensate for cell loss and to maintain a continuous epithelial layer with no gaps which has been observed in a model of RPE cell ablation [36]. On histological examination the lens and anterior portion of eye appeared normal in eyes lacking *Tmem98* but the retina was massively elongated and the choroid layer was compressed (Fig 3B). The eye globe was extremely structurally fragile with little integrity such that the eye folded on histological preparation and did not retain the normal globular shape (Fig 3B). We investigated the sclera by transmission electron microscopy but we did not observe any obvious abnormalities (S4 Fig). The retina was extremely thin and whilst all the layers of the retina appear to be present they were all reduced in thickness (Fig 3B). Measurements of retinal thickness from different regions of the eye showed that the reduction in retinal thickness was consistent throughout the retina (S5 Fig). The increase in eye size appears to be restricted to the posterior, retinal segment. From histological sections, including the optic nerve, we measured the circumference of mutant and control eyes. The total circumference of the mutant eyes (N=6) was greater than controls (N=8) (mean control 8218+/-352 μm, mean mutant 12289+/-1378 μm P= 0.007, unpaired two-tailed *t*-test). The circumferential length of the anterior segments of both groups of eyes was not significantly different (mean control 3287+/-273 μm, mean mutant 3165+/-351 μm P=0.79, unpaired two-tailed *t*-test) whereas the circumference of the posterior, retinal, segment of mutants was considerably greater (mean control 4931+/-215 μm, mean mutant 9124+/-1058 μm

P=0.0008, unpaired two-tailed *t*-test). We asked if the thinner retina was simply due to the expansion of the surface area of the globe. The increase in circumference of the retina corresponds to a ~2.9-fold increase in surface area (see Materials and Methods). By measuring the retina on the histological sections at six positions, three on each side of the optic nerve, we found the mean thickness of the mutant to be much smaller than controls (control 175.50+/-12.05 μm, mutant 61.75 +/- 5.21 μm, 6 measurements on 4 eyes for both). The ratio of control to mutant thickness is 2.84, consistent with the reduction in thickness being due to the same number of retinal cells spread over a larger area, although we cannot rule out the possibility that some degeneration and cell death has occurred. The number of photoreceptors, as indicated by the number of nuclei spanning the outer layer have also correspondingly decreased (control 11.9 +/-0.55, mutant 4.8 +/-0.32, 6 measurements on 4 eyes). Again the control to mutant ratio of 2.48 indicates that there is very little, if any, loss of photoreceptors.

At E17.5 some, but not all conditionally knocked-out eyes (1/3) had a similar elongated shape as observed in the complete knockout (S6A Fig) and by post-natal day (P)6 the increase in the size of the posterior segment and the thinning of the retina was apparent (S6B Fig), well before the eyes open at about P14 indicating that the disproportionate elongation and thinning of the retina mostly occurs in the immediate post-natal period.

Retinal function is severely impaired in *Tmem98* conditional knockout eyes

To assess retinal function we carried out electroretinography on control (n=3) and conditional mutant mice (n=3) at 6 months of age (Fig 4). The electroretinogram

(ERG) response was severely attenuated in the conditional mutant mice (Fig 4A). The amplitudes of both the a-wave, indicative of rod photoreceptor cell response to light stimulus, and the b-wave, indicative of the activation of Müller and bipolar cells were both greatly reduced (Fig 4A-C). These results suggest that there is a much diminished retinal response to light by the remaining thin retina in the conditional mutant mice.

Tmem98 conditional knockout eyes show signs of retinal stress

We next investigated the pattern of expression of glial fibrillary acidic protein (GFAP). GFAP is an intermediate filament protein that undergoes upregulation in the Müller cells in response to retinal stress, injury or damage [37]. In *Tmem98*$^{tm1c/tm1d}$ and *Tmem98*$^{tm1c/+}$; Tyr-Cre retinas we observed normal expression levels and localisation of GFAP whereas in the *Tmem98*$^{tm1c/\ tm1d}$; Tyr-Cre retina GFAP expression is increased and can be seen extending down to the outer nuclear layer of the retina indicating a stress response (Fig 5A). We stained retinal sections for EZRIN, an actin-binding protein located in the apical microvilli of the RPE and TMEM98 (Fig 5B). In *Tmem98* $^{tm1c/\ tm1d}$ and *Tmem98* $^{tm1c/+}$; Tyr-Cre retinas TMEM98 is present at both the apical and basolateral surfaces of the RPE. EZRIN staining can be seen at the apical surface of the RPE where it colocalises with TMEM98 as indicated by yellow staining at the apical surface of the RPE (Fig 5B). In the *Tmem98*$^{tm1c/\ tm1d}$; Tyr-Cre retina EZRIN is present but it is more diffuse and does not appear to be present in the apical microvilli. TMEM98 is not detected in the RPE confirming its deletion. We also stained retinal sections for the rod and cone opsins RHODOPSIN and ML-OPSIN (Fig 5C). The outer segments in the *Tmem98* $^{tm1c/\ tm1d}$; Tyr-Cre retina are

considerably shortened in comparison the *Tmem98*$^{tm1c/tm1d}$ and *Tmem98*$^{tm1c/+}$; Tyr-Cre retinas but both RHODOPSIN found in the rods and ML-OPSIN found in the cones are still present.

TMEM98 is a Type II transmembrane protein and interacts with MYRF

TMEM98 has been reported to be a single-pass type II transmembrane protein in which the C-terminal part is extracellular [10]. By Western blotting of ARPE-19 cells fractionated into the different cellular compartments we confirmed the membrane localisation of TMEM98 (Fig 6A). We confirmed the topology of the protein by assessing the accessibility to antibodies of N-terminal GFP and C-terminal V5 epitope tags fused to TMEM98 in transiently transfected NIH/3T3 cells (Fig 6B). In non-permeabilised cells only the V5 C-terminal tag was accessible confirming that the C-terminus is extracellular or luminal and the very short N-terminal end is cytoplasmic.

As a first step in determining the function of TMEM98 in the RPE and to understand why its absence results in eye expansion and thinning of the retina we sought to identify interacting proteins. To do this we carried out a proximity-dependent biotin identification (BioID) screen [38] in ARPE-19 cells. We chose to use this cell line because it is derived from retinal pigment epithelium and expresses *Tmem98* (Fig 6A). We made an expression construct where we fused a promiscuous biotin ligase (BirA*) domain to the C-terminal end of *Tmem98* and made a stably transfected ARPE-19 cell-line expressing this. We also made a stably transfected ARPE-19 control line expressing the BirA* domain alone. In the presence of biotin the BirA* promiscuously biotinylates proteins within a 10 nm radius. We extracted

protein from the cells, captured biotinylated proteins on streptavidin beads and subjected these to mass spectrometry analysis. We then compared the proteins isolated from the control and experimental cell lines. As expected TMEM98 was highly enriched in the experimental set indicating self-biotinylation (Fig 6C). A second protein, MYRF, had an even higher log2 fold change making it an excellent candidate for directly interacting with TMEM98 (Fig 6C). MYRF is an endoplasmic reticulum tethered transcription factor with a transmembrane domain near the C-terminal end of the protein. It assembles as a trimer and undergoes an autocatalytic cleavage reaction in an intramolecular chaperone domain that releases the N-terminal part of the protein which then translocates to the nucleus where it acts as a transcription factor important for oligodendrocyte specification and differentiation [39-42]. In all, 12 peptides derived from MYRF were found in the biotinylated fraction, nine from the N-terminal part and three from the C-terminal part. This suggested that either TMEM98 interacts with the full-length MYRF protein or with the two parts separately.

To test whether TMEM98 and MYRF directly interact we carried out co-immunoprecipitation experiments in HEK293T cells using TMEM98 tagged with V5 and MYRF, or a splice variant of MYRF lacking exon 19 (MYRFΔ19), tagged with MYC at the N-terminal end and FLAG at the C-terminal end. We tested the MYRFΔ19 splice form as well as the full-length as this is the predominant variant expressed in the RPE (B. Emery, personal communication and S7 Fig). When MYC-MYRF-FLAG or MYC-MYRFΔ19-FLAG was transfected alone the cleaved protein was detected by antibodies against MYC and FLAG but when transfected along with TMEM98-V5 the majority of the protein remained intact suggesting that TMEM98 inhibits the self-cleavage reaction (Fig 7A). After immunoprecipitation using anti-V5

antibodies both full-length and cleaved MYC-MYRF-FLAG or MYC-MYRFΔ19-FLAG could be detected by anti-FLAG antibodies but only the full-length protein could be detected by anti-MYC antibodies suggesting that TMEM98 interacts with the C-terminal part of MYRF (Fig 7A). We also stained transfected cells with antibodies against the epitope tags. TMEM98-V5 localises to the membrane when transfected alone or with MYC-MYRF-FLAG (Fig 7B, 7D). When transfected alone MYC-TMEM98-FLAG undergoes cleavage and the N-terminal part translocates to the nucleus and the C-terminal part colocalises with the membrane (Fig 7C). When transfected along with TMEM98-V5 the N-terminal portion of MYC-MYRF-FLAG is no longer detected in the nucleus but is found in the membrane along with the C-terminal portion and they colocalise with TMEM98-V5 (Fig 7D). We also tested two missense mutants of *Tmem98*, I135T and A193P, to ascertain if the ability of TMEM98 to inhibit MYRF self-cleavage was compromised by these mutations in co-transfection experiments (S8 Fig). The I135T missense mutation of *Tmem98* causes folds in the retinal layers which is accompanied by a retinal white spotting phenotype when heterozygous and is lethal when homozygous [15] and the A193P missense mutation is associated with dominant nanophthalmos in humans [6] and causes a recessive retinal phenotype in the mouse that is similar to the dominant phenotype caused by I135T [15]. Neither of these missense mutations affected the ability of TMEM98 to inhibit MYRF self-cleavage to any noticeable degree suggesting that the mutant phenotypes caused by these missense mutations are probably not due to a change in the interaction between TMEM98 and MYRF (S7 Fig).

MYRF is mislocalised in *Tmem98* Conditional Knockout Eyes

Both *Tmem98* and *Myrf* are reported to be highly expressed in the human and mouse RPE (http://www.biogps.org). We have confirmed the high expression of Tmem98 in the RPE (shown in Fig 1A, Fig 5 and S1 Fig) [15]. We anticipated that in mutant RPE, MYRF would be abnormally activated, and liberate the nuclear-localised portion of the protein. To examine the localisation of MYRF in normal RPE and RPE devoid of TMEM98 we stained RPE flat-mount preparations from *Tmem98*$^{1c/1d}$ and *Tmem98*$^{1c/1d}$; Tyr-Cre mice with antibodies directed against either the N-terminal or the C-terminal part of MYRF (Fig 8). In *Tmem98*$^{1c/1d}$ RPE we observed that the N-terminal portion of MYRF could be detected both in the membrane and the nucleus (Fig 8, top) and the C-terminal portion was found principally in the membrane. As we had previously shown by ZO1 staining (Fig 3A) the architecture of *Tmem98*$^{1c/1d}$; Tyr-Cre RPE lacking *Tmem98* is highly abnormal and the pattern of localisation of MYRF was altered with the increased immunostaining for the N-terminal portion of MYRF in the nucleus (Fig 8, bottom).

Discussion

In humans, mutations of *TMEM98* appear to cause dominant nanophthalmos [6, 7], whilst in population studies variants 5' of this gene are associated with myopia [2, 4, 5]. One of these variants, rs10512441, found 15 kb upstream of *TMEM98* is located in a region of active chromatin likely to have regulatory function [43]. We have shown here that loss of TMEM98 protein in the mouse, and specifically in the RPE, results in a greatly enlarged eye and a proportionally thinner retina. This excessive growth of the eye initiates before the mouse eyes are open, suggesting that the pathological changes we observe are not a result of the disruption of emmetropisation, the post-

natal mechanism of eye growth and corneal changes that in concert ensure that light is focused perfectly on the retina. The increased eye size is restricted to the posterior, retinal portion, leaving the anterior segment essentially unchanged. The posterior portion is enclosed by the RPE, and numerous studies point to the interaction between RPE and the surrounding sclera to be necessary for control of eye growth. However the mechanism by which the eye becomes enlarged is not simply loss of RPE function. Mutations which affect RPE function do not usually lead to alterations in eye size, rather the usual outcome is degeneration of the photoreceptors, for example loss-of-function of *RPE65* can lead to retinitis pigmentosa or leber congenital amaurosis [44, 45] and mutations in *C1QTNF5* can result in late-onset retinal macular degeneration [46]. Surprisingly, in our model we do not see substantial loss of photoreceptors. However, the reduced ERG response of the eyes where *Tmem98* has been knocked out indicates that they may have diminished function. The fragility of the mutant eyes during processing for histology suggests that the sclera is greatly weakened. However, on examination of the sclera by transmission electron microscopy we do not observe any obvious abnormalities (S4 Fig). Nanophthalmos is associated with a thickened sclera, and it is possible that the cause of *TMEM98* associated nanophthalmos involves misregulation of the same pathway which leads to weaker sclera in this loss-of-function model.

Loss-of-function of *Tmem98* in the RPE results in eye enlargement whereas missense mutations that cause dominant nanophthalmos in humans result in retinal defects when homozygous in the mouse but no significant change in eye size [15]. We proposed that the mode of action of the missense mutations was a dose-dependent gain-of-function because compound heterozygous mice with one missense allele and one deletion allele are viable with no eye phenotype. The

358 divergent consequences of mutations or variants on eye size is seen at other loci.
359 *PRSS56* is another human gene in which mutations can cause recessive
360 nanophthalmos [26, 47, 48] and variants of this gene are also associated with
361 myopia [2, 3].

362 The interaction between TMEM98 and MYRF has been shown by others [28,
363 49]. We confirmed the interaction using a proximity modification technique, which
364 does not necessarily rely on direct interaction, but we went on to demonstrate a
365 direct interaction does indeed occur (Fig 7). The interaction inhibits the self-cleavage
366 of MYRF and causes retention in the membrane, and is a novel mechanism of
367 regulation. We can show that in the absence of TMEM98, MYRF is ectopically
368 activated in the RPE and this may lead to aberrant gene regulation underlying the
369 large eye phenotype. Interestingly, heterozygous mutations of *MYRF* in humans lead
370 to nanophthalmos [28-31], suggesting loss of this protein has the opposite effect to
371 the activation we suggest occurs in the *Tmem98* deletion eyes. However, no
372 associations have been described in genome wide association studies between
373 *MYRF* and myopia or any other eye disorder. RPE-specific deletion of MYRF in the
374 mouse RPE does not lead to change in eye size but rather results in depigmentation
375 of the RPE [28]. This study also found that when *Myrf* expression is reduced in the
376 eye a reduction in *Tmem98* transcription results accompanied by severely reduced
377 detection of TMEM98 protein in the RPE. In spite of this depletion of TMEM98 the
378 architecture of the RPE is unaltered in stark contrast to the highly aberrant RPE in
379 the *Tmem98*$^{tm1c/tm1d}$; TyrCre mice where only *Tmem98* is deleted (Fig 2D and Fig
380 3A). This suggests that in our experiment the eye size phenotype associated with
381 loss of TMEM98 requires functional MYRF, further implicating dysregulation of
382 MYRF in the mechanism and that the sequestration of MYRF at the endoplasmic

reticulum occurs under physiological conditions and is not an artefact caused by overexpression. It would be interesting to determine the eye phenotype when *Myrf* is deleted as well as *Tmem98* in the RPE. A prediction might be that the enlarged eye phenotype would be rescued.

In summary, mouse mutagenesis provides a useful means of validating candidate genes identified through GWAS studies, and addressing the mechanism of action and pathways involved.

Materials and Methods

Mice

All experiments with mice complied with United Kingdom Home Office regulations, were performed under United Kingdom Home Office project licence approval were in accordance with the ARVO Statement for the Use of Animals in Ophthalmic and Vision Research. Clinical examinations were carried out as previously described [50]. Fundus imaging was performed as described [51]. Mice carrying a targeted knockout-first conditional-ready allele of *Tmem98*, *Tmem98*$^{tm1a(EUCOMM)Wtsi}$ (hereafter *Tmem98*^{tm1a}), were obtained from the Sanger Institute. By crossing *Tmem98*$^{tm1a/+}$ mice with mice carrying a germ-line Cre the "knockout-first" *tm1a* allele is converted to the reporter knockout allele *Tmem98*$^{tm1b(EUCOMM)Wtsi}$ (hereafter *Tmem98*^{tm1b} or *Tmem98*^{1b}) . By crossing *Tmem98*$^{tm1a/+}$ mice with mice carrying FLPe the *Tmem98*^{tm1a} 'knockout-first' allele was converted to the floxed conditional allele *Tmem98*$^{tm1c(EUCOMM)Wtsi}$ (hereafter *Tmem98*^{tm1c} or *Tmem98*^{1c}). By crossing *Tmem98*$^{tm1c/+}$ mice with mice carrying Cre the floxed critical exon 4 is deleted in cells expressing Cre generating a deletion allele that has a frame shift

Tmem98$^{tm1d(EUCOMM)Wtsi}$ (hereafter *Tmem98*^{tm1d} or *Tmem98*^{1d}) that would be subject to nonsense mediated decay [52]. FLPe expressing mice were made by Andrew Smith, University of Edinburgh [53]. Germ-line Cre expressing mice were made by Dirk Kleinjan, MRC Human Genetics Unit [54]. Tyr-Cre expressing mice were originally obtained from Lionel Larue, Institut Pasteur [33] and R26MTMG mice reporter mice were originally obtained from Liqun Luo, Stanford University [34]. Mice were initially genotyped by PCR using the primers listed in S1 Table and subsequently by Transnetyx (Cordova, TN, USA) using custom designed assays (http://www.transnetyx.com). All mouse lines were maintained on the C57BL/6J mouse strain background.

Electroretinography

Before testing mice were dark-adapted overnight (>16 hours) and electroretinography was carried out in a darkened room under red light illumination using an HMsERG system (Ocuscience, Henderson, MV, US). Mice were anaesthetised with isofluorane and their pupils dilated with 1% tropicamide. Three grounding electrodes were placed subcutaneously, in the base of the body above the tail and each cheek, and silver-coated electrodes were positioned concentrically on the corneas with hypromellose eye drops (2.5% methylcellulose coupling agent) held in place with contact lenses. Mice were placed on a heated platform to maintain their body temperature at 37°C and monitored with a rectal thermometer. A modified QuickRetCheck (Ocuscience) protocol was used to obtain full-field scotopic ERGs. Briefly, four flashes at 10 mcd.s/m^2 at two second intervals were followed by four

flashes at 3 mcd.s/m^2 at ten second intervals and then by four flashes at 10 mcd.s/m^2 at ten second intervals.

Confocal scanning laser ophthalmoscope (cSLO) and optical coherence tomography (OCT) imaging

Imaging was performed using a Spectralis OCT plus MultiColor, confocal scanning laser ophthalmoscope (Heidelberg Engineering, Heidelberg, Germany). Mice were anesthetised via intraperitoneal injection of ketamine (80 mg/kg body weight, Vetalar; Zoetis UK Limited, Leatherhead, Surrey, UK) and xylazine (10 mg/kg body weight, Rompun; Bayer PLC, Reading, Berkshire, UK) diluted in sterile 0.9% saline solution. Pupils were dilated with tropicamide 1% and phenylephrine hydrochloride 2.5% eye drops (both Bausch & Lomb, Kingston upon Thames, UK). In wild-type mice, a custom-made polymethylmethacrylate (PMMA) contact lens was placed on the cornea with 0.3% methylcellulose gel as viscous coupling fluid. SLO images were recorded using IR (infrared) reflectance, blue-light autofluorescence (BAF), IR autofluorescence (IRAF) and multicolour reflectance imaging modes. IR reflectance was used as a reference imaging to perform spectral-domain (SD)-OCT. The SD-OCT scans were acquired using volume protocols provided by the Spectralis software, orientated such that their superior and inferior sectors were positioned over the optic nerve head. Total retinal thickness was automatically calculated using the Heidelberg software. The longer/larger eye size in mutant mice meant that images could not be recorded using the same custom-made PMMA contact lens as above. Instead a flat, glass, 6mm-diameter round coverslip was used on a drop of 2% w/w polyacrylic acid gel (Viscotears, Bausch & Lomb, Kingston upon Thames, UK)

454 placed on the cornea. Images were recorded using “automatic real time” (ART)
455 mode, which tracks ocular movement (e.g., due to respiration) and averages
456 consecutive images resulting in an improved signal-to-noise ratio. At least 25
457 images/OCT b-scans were averaged, except in the case of IRAF mode imaging in
458 mutant mice, where the signal was too low to mediate tracking, and a single image
459 was used.

460

461 **Histology and immunohistochemistry**

462 Mice were culled by cervical dislocation, eyes enucleated and fixed in Davidson’s
463 fixative (28.5% ethanol, 2.2% neutral buffered formalin, 11% glacial acetic acid) for 1
464 hour at room temperature (cryosectioning) or more than 16 hours at 4°C (wax
465 embedding). Embryos, following dissection and removal of a tail sample to be used
466 for genotyping, were fixed in Davidson’s fixative at 4°C. Before wax embedding fixed
467 tissue was dehydrated through an ethanol series. Haematoxylin and eosin (H&E)
468 staining was performed on 5-10 µm paraffin embedded tissue sections using
469 standard procedures and images captured using a Nanozoomer XR scanner
470 (Hamamatsu, Hamamatsu City, Japan) and viewed using NDP.view2 software
471 (Hamamatsu). For cryosectioning, fixed tissue was transferred to 5% sucrose in
472 phosphate buffered saline (PBS) and once sunk transferred to 20% sucrose in PBS
473 overnight. Samples were then embedded in OCT compound on dry ice and
474 cryosectioned at 14 µM. For immunostaining on cryosections, slides were washed
475 with water and post-fixed in acetone at -20°C for 10 minutes. They were then rinsed
476 with water, blocked in 10% heat-inactivated donkey serum (DS) in Tris-HCl buffered
477 saline (TBS) with 0.1% Tween-20 in (TBST) for one hour and then incubated with

primary antibodies diluted in TBST with 5% DS for two hours at room temperature or overnight at 4°C. Subsequently, after washing with TBST, the slides were incubated with Alexa Fluor secondary antibodies (Invitrogen, Carlsbad, CA, USA) diluted 1:400 in TBST with 5% DS at room temperature for one hour. Following washing with TBST coverslips were mounted on slides in Prolong Gold (Thermo Fisher Scientific, Waltham, MA, USA) and confocal images acquired on a Nikon Confocal A1R microscope (Nikon Instruments, Tokyo, Japan). The microscope comprises of a Nikon Eclipse TiE inverted microscope with Perfect Focus System and is equipped with 405nm diode, 457/488/514nm Multiline Argon, 561nm DPSS and 638nm diode lasers. Data were acquired using NIS Elements AR software (Nikon Instruments). Images were processed using either NIS-Elements or ImageJ software [55].

Eye size measurements

The circumference of control and mutant eyes was measured from H&E stained histological sections through the optic nerve using NDP.view2 software (Hamamatsu). To compare the retinal surface areas we treated the eye as a sphere, and calculated the radius, R, and the total surface area from the circumference. We then calculated the surface area of the anterior (non-retinal) portion by treating this as a spherical cap, determining the cap angle, θ, from the fraction of the total circumference enclosed by the anterior segment, hence the cap radius, r, as equal to $R\sin\theta$ and the height of the cap, h, as equal to $R-\sqrt{(R^2-r^2)}$. The surface area of the cap is $= \pi(r^2+h^2)$ and hence the surface area of the retina is the total surface minus the cap area.

RPE flat mounts

Immunohistochemistry on RPE flat mount was carried out as previously described [56]. Briefly, eyes were enucleated and the cornea, lens and retina removed. The RPE was dissected, radial incisions were made in the periphery to allow it to flatten, and it was fixed in cold (-20°C) methanol for a minimum of 30 minutes. After rehydration in PBS RPE was blocked in whole mount buffer (PBS containing 3% Triton X-100, 0.5% Tween-20 and 1% bovine serum albumin (BSA)) which was also used for all washing and antibody incubation steps. After blocking RPE was incubated with primary antibodies overnight at 4°C, washed and then incubated with secondary antibodies for two hours at room temperature and then washed, mounted in Prolong Gold (Thermo Fisher Scientific) and imaged as above.

LacZ staining

For LacZ staining of cryosections slides were stained overnight in detergent buffer (0.1 M phosphate buffer pH7.3, 2 mM $MgCl_2$, 0.1% sodium deoxycholate and 0.02% NP-40 (IGEPAL CA-630)) containing 14.5 mM NaCl, 5 mM $K_3Fe(CN)_6$, 5 mM $K_4[Fe(CN)_6].3H_20$ and 150 µg X-gal (5-bromo-4-chloro-3-indolyl-β-D-galactopyranoside) in a coplin jar at 37°C protected from light. They were then washed twice in detergent buffer, post-fixed overnight in 4% paraformaldehyde (PFA) in PBS, counterstained with eosin and mounted using standard procedures. Brightfield images were acquired using a QImaging R6 colour CCD camera (QImaging, Surrey, BC, Canada) mounted on a Zeiss Axioplan II fluorescence microscope with Plan-neofluar or Plan Apochromat objectives (Carl Zeiss,

525 Oberkocken, Germany). Image capture was performed using Micromanager
526 (https://open-imaging.com/).

527

528 **Cell culture and transfection and stable cell line generation**

529 NIH/3T3 and HEK293T cells were grown in DMEM (Thermo Fisher Scientific)
530 supplemented with 10% fetal calf serum (FCS) and 1% penicillin/streptomycin.
531 ARPE-19 cells were grown in DMEM:F12 (Thermo Fisher Scientific) supplemented
532 with 10% FCS and 1% penicillin/streptomycin. All cells were grown in a humidified
533 5% CO_2 incubator at 37°C. Cell transfection was carried out using a Neon
534 Transfection System (Invitrogen) following the manufacturer's instructions except for
535 the topology experiment described below. The optimal concentration of G418
536 antibiotic (Sigma-Aldrich, St. Louis, MO, USA) to kill ARPE-19 cells was determined
537 by a kill curve using standard procedures
538 (https://www.mirusbio.com/applications/stable-cell-line-generation/antibiotic-kill-
539 curve) and G418 was used at a concentration of 0.8 mg/ml for generation and
540 culture of stable cell lines. For generation of stable ARPE-19 cell lines, HEK293T
541 cells were transiently transfected with pGAG/POL (gift from Tannishtha Reya
542 (Addgene plasmid #14887) and pMD2.G (gift from Didier Trono (Addgene plasmid
543 #12259) plus pQCXIN-BirA plasmids using Fugene HD (Promega, Madison, WI,
544 USA). Virus-containing medium was collected, filtered through a 0.4 µm filter and
545 mixed with an equal volume of fresh culture medium. Polybrene (Thermo Fisher
546 Scientific) was added to 4 µg/ml and virus added to sub-confluent ARPE-19 cells. 12
547 hours later, medium was replaced. 48 hours after infection, stable expressing pools
548 were selected using medium containing 0.8 mg/ml G418 (Thermo Fisher Scientific).

Plasmids

To generate retroviral constructs for BioID experiments, the BirA-R118G open reading frame from the BirA(R118G)-HA destination vector (gift from Karl Kramer (plasmid # 53581, http://www.addgene.org) was subcloned into the retroviral vector pQCXIN (Clontech) to generate either N-terminal (pQCXIN-BirA-Myc-N) or C-terminal (pQCXIN-BirA-Myc-C) vectors. Full-length *Tmem98* without the stop codon was amplified by polymerase chain reaction (PCR) with the following primers: 5'-GGTTCCGTACGATGGAGACTGTGGTGATCGTC-3' and 5'-GGTTCGGATCCAATGGCCGACTGTTCCTGCAGG-3' which placed a BsiWI site at the 5' end and a BamHI site at the 3' end. This was cloned into the BsiWI and BamHI sites of the expression vector pQCXIN-BirA-Myc-C so that a BirA* domain was fused to the C-terminal of TMEM98. Other *Tmem98* expression constructs were made using the Gateway Cloning System (Thermo Fisher Scientific). The *Tmem98* open reading frame without the initiating ATG was amplified by PCR using primers 5'-CACCGAGACTGTGGTGATCGTCG-3' and 5'- AATGGCCGACTGTTCCTGCAG-3' and cloned into pENTR™/D-TOPO™ (Thermo Fisher Scientific) and subsequently into pcDNA™6.2/N-EmGFP-DEST (Thermo Fisher Scientific) to create GFP-Tmem98-V5, fusing a GFP tag at the N-terminal end of TMEM98 and a V5 tag at the C-terminal end. The *Tmem98* open reading frame with the initiating ATG was amplified by PCR using the primers 5'- CACCATGGAGACTGTGGTGATCGTCG-3' and 5'- AATGGCCGACTGTTCCTGCAG-3' and cloned into pENTR™/D-TOPO™ (Thermo Fisher Scientific) and subsequently into pcDNA™-DEST40 (Thermo Fisher Scientific) to create TMEM98-V5, fusing a V5 tag at the C-terminal end of TMEM98. MYC-MYRF-FLAG and MYC-MYRFΔ19-FLAG have been described [39].

574

575 **Immunocytochemistry**

576 Cells were grown on coverslips and fixed in 4% PFA/PBS for 10 minutes at room
577 temperature, washed with TBS containing 0.1% Triton X-100 (TBSTx). Cells were
578 blocked in 10% DS in TBSTx for one hour at room temperature. Primary antibodies
579 diluted in TBSTx/1% DS were then added and incubated for one hour at room
580 temperature or 4°C overnight. Following washing with TBSTx all cells were
581 incubated with Alexa Fluor secondary antibodies (Invitrogen) diluted 1:500 in
582 TBSTx/1% DS at room temperature for one hour. Cells were then washed with
583 TBSTx, incubated with 4′,6-diamidino-2-phenylindole (DAPI) at 2 µg/ml for five
584 minutes, washed again with TBSTx and then mounted on slides in Prolong Gold
585 (Thermo Fisher Scientific). Confocal images were acquired and processed as
586 described above.

587

588 **Topology of TMEM98**

589 GFP-Tmem98-V5 was transiently transfected into NIH/3T3 cells using Lipofectamine
590 2000 (Thermo Fisher Scientific) following the manufacturer's protocol and cells
591 grown overnight in chamber slides. For immunofluorescence on permeabilised cells
592 the cells were fixed in 4% PFA/PBS for 10 minutes, washed with TBSTx at room
593 temperature (RT) followed by blocking in DS in TBSTx for 30 minutes and then
594 incubated in primary antibodies diluted in TBSTx with 10% DS for one hour at 4°C.
595 For immunofluorescence on non-permeabilised cells the cells were washed with ice-
596 cold TBS, blocked in TBS with 10% DS for 10 minutes followed by incubation with
597 primary antibodies diluted in TBS with 10% DS for one hour, washed with TBS all at

598 4°C and then fixed as described above. Subsequently, after washing with TBSTx, all
599 cells were incubated with Alexa Fluor secondary antibodies (Invitrogen) diluted
600 1:1000 in TBSTx with 10% DS at room temperature for one hour. Following washing
601 with TBSTx the chamber was removed and coverslips were mounted on slides in
602 Prolong Gold (Thermo Fisher Scientific) and confocal images acquired and
603 processed as described above.

604

605 **Fractionation of ARPE-19 cells and Western blotting**

606 ARPE-19 cells were separated into cytoplasmic, membrane/organelle and
607 nuclear/cytoskeletal fractions using the Cell Fractionation Kit (Cell Signaling
608 Technology, Danvers, MA, USA) following the manufacturer's instructions. For
609 Western blotting, fractions or equal amounts of protein lysates were separated on
610 either 4-12% or 12% NuPAGE Bis-Tris gels (Thermo Fisher Scientific) depending on
611 the size of the protein of interest and transferred to polyvinylidene difluoride (PVDF)
612 or nitrocellulose membranes. Membranes were blocked for one hour at room
613 temperature in SuperBlock T20 (TBS) Blocking Buffer (Thermo Fisher Scientific) and
614 incubated with primary antibodies for one hour at room temperature or overnight at
615 4°C in blocking buffer with shaking. Following washing with TBST membranes were
616 incubated with ECL horse radish peroxidase (HRP)-conjugated secondary antibodies
617 (GE Healthcare, Chicago, IL, USA) diluted 1:5000 in blocking buffer for one hour at
618 room temperature, washed with TBST and developed using SuperSignal™ West
619 Pico PLUS (Thermo Fisher Scientific).

620

621 **BioID experiment and mass spectrometry**

ARPE-19 stable cell lines expressing TMEM98 tagged with BirA* fusion protein or BirA* alone were cultured in three 15 cm plates until 70-80% confluent. The culture medium was then replaced with medium containing 50 mM biotin and cultured for a further 24 hours when the cells were lysed using RIPA Buffer (Cell Signaling Technology) with 1 µM phenylmethylsulfonyl fluoride (PMSF) (Sigma-Aldrich) and Complete Protease Inhibitor Cocktail (Roche, Basel, Switzerland) following the manufacturer's instructions. Lysates were diluted in RIPA buffer with 1 µM PMSF and Complete Protease Inhibitor Cocktail (Roche) to a concentration of 1.68 mg/ml and 500 µl was used for capture of biotinylated proteins on streptavidin beads and subsequent mass spectrometry analysis. Streptavidin beads were diluted in IP buffer so that the equivalent of 5 beads were used per sample. Beads were transferred using a Thermo Kingfisher Duo into 500 µl lysate and incubated for one hour with mixing. All steps are at 5°C unless otherwise stated. Beads were then transferred for two washes in IP buffer and three washes in TBS (300 µl each). After transfer into 100 µl 2M urea, 100 mM Tris, 1 mM DTT containing 0.3 µg trypsin per sample, beads were incubated at 27°C for 30 minutes with mixing to achieve limited proteolysis. The beads were then removed and tryptic digest of the released peptides was allowed to continue for 9 hours at 37°C. Following this, peptides were alkylated by adding iodoacetamide to 50 mM and incubating at room temperature for 30 minutes. Finally, peptides were acidified by addition of 8 µl 10% TFA. An estimated 10 µg of the resulting peptide solution was loaded onto an activated (20 µl methanol), equilibrated (50 µl 0.1% TFA) C18 StAGE tip, and washed with 50 µl 0.1% trifluoroacetic acid (TFA). The bound peptides were eluted into a 96-well plate (Axygen, Corning Inc., Corning, NY, USA) with 20 µl 80% acetonitrile (ACN), 0.1% TFA and concentrated to less than 4 µl in a vacuum concentrator. The final volume

was adjusted to 15 µl with 0.1% TFA. Online LC was performed using a Dionex RSLC Nano (Thermo Fisher Scientific). Following the C18 clean-up, 5 µg peptides were injected onto a C18 packed emitter and eluted over a gradient of 2%-80% ACN in 48 minutes, with 0.5% acetic acid throughout. Eluting peptides were ionised at +2.2kV before data-dependent analysis on a Thermo Q-Exactive Plus. MS1 was acquired with mz range 300-1650 and resolution 70,000, and top 12 ions were selected for fragmentation with normalised collision energy of 26, and an exclusion window of 30 seconds. MS2 were collected with resolution 17,500. The AGC targets for MS1 and MS2 were 3e6 and 5e4 respectively, and all spectra were acquired with 1 microscan and without lockmass. Finally, the data were analysed using MaxQuant (v 1.5.6.5) (max planck institute of biochemistry) in conjunction with uniprot human reference proteome release 2016_11 (https://www.uniprot.com), with match between runs (MS/MS not required), LFQ with 1 peptide required, and statistical analyses performed in R (RStudio 1.1.453 / R x64 3.4.4) (https://rstudio.com) using Wasim Aftab's LIMMA Pipeline Proteomics (https://github.com/wasimaftab/LIMMA-pipeline-proteomics) implementing a Bayes-moderated method [57].

Co-immunoprecipitation

HEK293T cells cultured in 100 mm dishes were transfected with 5 µg of each expression plasmid as indicated. After 24 hours the cells were lysed using Cell Lysis Buffer (Cell Signaling Technology) with 1 µM PMSF and Complete Protease Inhibitor Cocktail (Roche) following the manufacturer's instructions. Lysates were incubated with anti-V5 agarose affinity gel (Sigma-Aldrich) at 4°C overnight with agitation. The agarose affinity gel was then washed three times with Cell Lysis Buffer (Cell

671 Signaling Technology) and bound proteins eluted with NuPAGE LDS Sample Buffer
672 (Thermo Fisher Scientific) with NuPAGE Sample Reducing Agent (Thermo Fisher
673 Scientific) by incubating at 70°C for 10 minutes and separated on 4-12% NuPAGE
674 Bis-Tris gels (Thermo Fisher Scientific) along with 5% of input samples and analysed
675 by Western blotting as described above.

676

677 **Statistics**

678 Statistical analysis was carried out using the program Graphpad Prism (Graphpad
679 Software, San Diego, CA, USA). The statistical test used is indicated in the text. A
680 value of $P<0.05$ was considered significant.

681

682 **Acknowledgements**

683 The authors thank IGMM scientific support services, Craig Nicol and Conor Warnock
684 for help with photography, the IGMM Advanced Imaging Resource for help with
685 imaging and Edinburgh University Bioresearch and Veterinary Services for animal
686 husbandry. The authors are very grateful to Michael Wegner for the gift of anti-MYRF
687 (N-terminal) antibody, Ben Emery and Biliana Veleva-Rotse for the gifts of anti-
688 MYRF (C-terminal) antibody and MYRF expression constructs and Ben Emery for
689 helpful comments on the manuscript. Also Tannishtha Reya, Didier Trono and Karl
690 Kramer for the gifts of plasmids.

691 **References**

692 1. Wojciechowski R. Nature and nurture: the complex genetics of myopia and refractive error.
693 Clinical genetics. 2011;79(4):301-20. Epub 2010/12/16. doi: 10.1111/j.1399-0004.2010.01592.x.
694 PubMed PMID: 21155761; PubMed Central PMCID: PMCPMC3058260.

2. Kiefer AK, Tung JY, Do CB, Hinds DA, Mountain JL, Francke U, et al. Genome-wide analysis points to roles for extracellular matrix remodeling, the visual cycle, and neuronal development in myopia. PLoS genetics. 2013;9(2):e1003299.
3. Verhoeven VJ, Hysi PG, Wojciechowski R, Fan Q, Guggenheim JA, Hohn R, et al. Genome-wide meta-analyses of multiancestry cohorts identify multiple new susceptibility loci for refractive error and myopia. Nat Genet. 2013;45(3):314-8. PubMed PMID: 23396134.
4. Tedja MS, Wojciechowski R, Hysi PG, Eriksson N, Furlotte NA, Verhoeven VJM, et al. Genome-wide association meta-analysis highlights light-induced signaling as a driver for refractive error. Nat Genet. 2018;50(6):834-48. Epub 2018/05/29. doi: 10.1038/s41588-018-0127-7. PubMed PMID: 29808027; PubMed Central PMCID: PMCPMC5980758.
5. Pickrell JK, Berisa T, Liu JZ, Segurel L, Tung JY, Hinds DA. Detection and interpretation of shared genetic influences on 42 human traits. Nat Genet. 2016;48(7):709-17. Epub 2016/05/18. doi: 10.1038/ng.3570. PubMed PMID: 27182965; PubMed Central PMCID: PMCPMC5207801.
6. Awadalla MS, Burdon KP, Souzeau E, Landers J, Hewitt AW, Sharma S, et al. Mutation in TMEM98 in a large white kindred with autosomal dominant nanophthalmos linked to 17p12-q12. JAMA ophthalmology. 2014;132(8):970-7. Epub 2014/05/24. doi: 10.1001/jamaophthalmol.2014.946. PubMed PMID: 24852644.
7. Khorram D, Choi M, Roos BR, Stone EM, Kopel T, Allen R, et al. Novel TMEM98 mutations in pedigrees with autosomal dominant nanophthalmos. Molecular vision. 2015;21:1017-23. Epub 2015/09/24. PubMed PMID: 26392740; PubMed Central PMCID: PMCPMC4556162.
8. Imadome K, Iwakawa M, Nakawatari M, Fujita H, Kato S, Ohno T, et al. Subtypes of cervical adenosquamous carcinomas classified by EpCAM expression related to radiosensitivity. Cancer biology & therapy. 2010;10(10):1019-26. Epub 2010/09/22. doi: 10.4161/cbt.10.10.13249. PubMed PMID: 20855955.
9. Ng KT, Lo CM, Guo DY, Qi X, Li CX, Geng W, et al. Identification of transmembrane protein 98 as a novel chemoresistance-conferring gene in hepatocellular carcinoma. Molecular cancer therapeutics. 2014;13(5):1285-97. Epub 2014/03/13. doi: 10.1158/1535-7163.mct-13-0806. PubMed PMID: 24608572.
10. Fu W, Cheng Y, Zhang Y, Mo X, Li T, Liu Y, et al. The Secreted Form of Transmembrane Protein 98 Promotes the Differentiation of T Helper 1 Cells. Journal of interferon & cytokine research : the official journal of the International Society for Interferon and Cytokine Research. 2015;35(9):720-33. Epub 2015/05/07. doi: 10.1089/jir.2014.0110. PubMed PMID: 25946230; PubMed Central PMCID: PMCPMC4560856.
11. Mao M, Chen J, Li X, Wu Z. siRNA-TMEM98 inhibits the invasion and migration of lung cancer cells. International journal of clinical and experimental pathology. 2015;8(12):15661-9. Epub 2016/02/18. PubMed PMID: 26884835; PubMed Central PMCID: PMCPMC4730048.
12. Lv G, Zhu H, Li C, Wang J, Zhao D, Li S, et al. Inhibition of IL-8-mediated endothelial adhesion, VSMCs proliferation and migration by siRNA-TMEM98 suggests TMEM98's emerging role in atherosclerosis. Oncotarget. 2017;8(50):88043-58. Epub 2017/11/21. doi: 10.18632/oncotarget.21408. PubMed PMID: 29152140; PubMed Central PMCID: PMCPMC5675692.
13. Tang Q, Ran H. MicroRNA-219-5p inhibits wound healing by targeting TMEM98 in keratinocytes under normoxia and hypoxia condition. European review for medical and pharmacological sciences. 2018;22(19):6205-11. Epub 2018/10/20. doi: 10.26355/eurrev_201810_16026. PubMed PMID: 30338788.
14. Bliss SA, Paul S, Pobiarzyn PW, Ayer S, Sinha G, Pant S, et al. Evaluation of a developmental hierarchy for breast cancer cells to assess risk-based patient selection for targeted treatment. Sci Rep. 2018;8(1):367. Epub 2018/01/13. doi: 10.1038/s41598-017-18834-5. PubMed PMID: 29321622; PubMed Central PMCID: PMCPMC5762675.
15. Cross SH, McKie L, Keighren M, West K, Thaung C, Davey T, et al. Missense Mutations in the Human Nanophthalmos Gene TMEM98 Cause Retinal Defects in the Mouse. Investigative

ophthalmology & visual science. 2019;60(8):2875-87. Epub 2019/07/03. doi: 10.1167/iovs.18-25954. PubMed PMID: 31266059.

16. Marmorstein LY, Wu J, McLaughlin P, Yocom J, Karl MO, Neussert R, et al. The light peak of the electroretinogram is dependent on voltage-gated calcium channels and antagonized by bestrophin (best-1). The Journal of general physiology. 2006;127(5):577-89.

17. Milenkovic A, Brandl C, Milenkovic VM, Jendryke T, Sirianant L, Wanitchakool P, et al. Bestrophin 1 is indispensable for volume regulation in human retinal pigment epithelium cells. Proceedings of the National Academy of Sciences. 2015;112(20):E2630-E9.

18. Zhang Y, Stanton JB, Wu J, Yu K, Hartzell HC, Peachey NS, et al. Suppression of Ca 2+ signaling in a mouse model of Best disease. Human molecular genetics. 2010;19(6):1108-18.

19. Mehalow AK, Kameya S, Smith RS, Hawes NL, Denegre JM, Young JA, et al. CRB1 is essential for external limiting membrane integrity and photoreceptor morphogenesis in the mammalian retina. Human molecular genetics. 2003;12(17):2179-89.

20. van de Pavert SA, Kantardzhieva A, Malysheva A, Meuleman J, Versteeg I, Levelt C, et al. Crumbs homologue 1 is required for maintenance of photoreceptor cell polarization and adhesion during light exposure. Journal of Cell Science. 2004;117(18):4169-77.

21. van de Pavert SA, Meuleman J, Malysheva A, Aartsen WM, Versteeg I, Tonagel F, et al. A single amino acid substitution (Cys249Trp) in Crb1 causes retinal degeneration and deregulates expression of pituitary tumor transforming gene Pttg1. Journal of Neuroscience. 2007;27(3):564-73.

22. Fogerty J, Besharse JC. 174delG mutation in mouse MFRP causes photoreceptor degeneration and RPE atrophy. Investigative ophthalmology & visual science. 2011;52(10):7256-66.

23. Kameya S, Hawes NL, Chang B, Heckenlively JR, Naggert JK, Nishina PM. Mfrp, a gene encoding a frizzled related protein, is mutated in the mouse retinal degeneration 6. Human molecular genetics. 2002;11(16):1879-86.

24. Hawes NL, Chang B, Hageman GS, Nusinowitz S, Nishina PM, Schneider BS, et al. Retinal degeneration 6 (rd6): a new mouse model for human retinitis punctata albescens. Investigative ophthalmology & visual science. 2000;41(10):3149-57.

25. Velez G, Tsang SH, Tsai Y-T, Hsu C-W, Gore A, Abdelhakim AH, et al. Gene Therapy Restores Mfrp and Corrects Axial Eye Length. Scientific Reports. 2017;7(1):16151. doi: 10.1038/s41598-017-16275-8.

26. Nair KS, Hmani-Aifa M, Ali Z, Kearney AL, Salem SB, Macalinao DG, et al. Alteration of the serine protease PRSS56 causes angle-closure glaucoma in mice and posterior microphthalmia in humans and mice. Nature Genetics. 2011;43:579. doi: 10.1038/ng.813.

27. Paylakhi S, Labelle-Dumais C, Tolman NG, Sellarole MA, Seymens Y, Saunders J, et al. Muller glia-derived PRSS56 is required to sustain ocular axial growth and prevent refractive error. PLoS Genet. 2018;14(3):e1007244. PubMed PMID: 29529029.

28. Garnai SJ, Brinkmeier ML, Emery B, Aleman TS, Pyle LC, Veleva-Rotse B, et al. Variants in myelin regulatory factor (MYRF) cause autosomal dominant and syndromic nanophthalmos in humans and retinal degeneration in mice. PLoS Genet. 2019;15(5):e1008130. Epub 2019/05/03. doi: 10.1371/journal.pgen.1008130. PubMed PMID: 31048900.

29. Guo C, Zhao Z, Chen D, He S, Sun N, Li Z, et al. Detection of Clinically Relevant Genetic Variants in Chinese Patients With Nanophthalmos by Trio-Based Whole-Genome Sequencing Study. Investigative ophthalmology & visual science. 2019;60(8):2904-13. Epub 2019/07/03. doi: 10.1167/iovs.18-26275. PubMed PMID: 31266062.

30. Xiao X, Sun W, Ouyang J, Li S, Jia X, Tan Z, et al. Novel truncation mutations in MYRF cause autosomal dominant high hyperopia mapped to 11p12-q13.3. Human genetics. 2019;138(10):1077-90. Epub 2019/06/07. doi: 10.1007/s00439-019-02039-z. PubMed PMID: 31172260; PubMed Central PMCID: PMCPMC6745028.

31. Siggs OM, Souzeau E, Breen J, Qassim A, Zhou T, Dubowsky A, et al. Autosomal dominant nanophthalmos and high hyperopia associated with a C-terminal frameshift variant in MYRF.

795 Molecular vision. 2019;25:527-34. Epub 2019/11/09. PubMed PMID: 31700225; PubMed Central
796 PMCID: PMCPMC6817736.
797 32. Kluppel M, Beermann F, Ruppert S, Schmid E, Hummler E, Schutz G. The mouse tyrosinase
798 promoter is sufficient for expression in melanocytes and in the pigmented epithelium of the retina.
799 Proceedings of the National Academy of Sciences of the United States of America. 1991;88(9):3777-
800 81. Epub 1991/05/01. doi: 10.1073/pnas.88.9.3777. PubMed PMID: 1902569; PubMed Central
801 PMCID: PMCPMC51536.
802 33. Delmas V, Martinozzi S, Bourgeois Y, Holzenberger M, Larue L. Cre-mediated recombination
803 in the skin melanocyte lineage. Genesis (New York, NY : 2000). 2003;36(2):73-80. Epub 2003/06/24.
804 doi: 10.1002/gene.10197. PubMed PMID: 12820167.
805 34. Muzumdar MD, Tasic B, Miyamichi K, Li L, Luo L. A global double-fluorescent Cre reporter
806 mouse. Genesis (New York, NY : 2000). 2007;45(9):593-605. Epub 2007/09/18. doi:
807 10.1002/dvg.20335. PubMed PMID: 17868096.
808 35. Stevenson BR, Siliciano JD, Mooseker MS, Goodenough DA. Identification of ZO-1: a high
809 molecular weight polypeptide associated with the tight junction (zonula occludens) in a variety of
810 epithelia. The Journal of cell biology. 1986;103(3):755-66. Epub 1986/09/01. doi:
811 10.1083/jcb.103.3.755. PubMed PMID: 3528172; PubMed Central PMCID: PMCPMC2114282.
812 36. Longbottom R, Fruttiger M, Douglas RH, Martinez-Barbera JP, Greenwood J, Moss SE.
813 Genetic ablation of retinal pigment epithelial cells reveals the adaptive response of the epithelium
814 and impact on photoreceptors. Proceedings of the National Academy of Sciences of the United
815 States of America. 2009;106(44):18728-33. Epub 2009/10/24. doi: 10.1073/pnas.0902593106.
816 PubMed PMID: 19850870; PubMed Central PMCID: PMCPMC2765920.
817 37. Lewis GP, Fisher SK. Up-regulation of glial fibrillary acidic protein in response to retinal
818 injury: its potential role in glial remodeling and a comparison to vimentin expression. International
819 review of cytology. 2003;230:264-90.
820 38. Roux KJ, Kim DI, Raida M, Burke B. A promiscuous biotin ligase fusion protein identifies
821 proximal and interacting proteins in mammalian cells. The Journal of cell biology. 2012;196(6):801-
822 10. Epub 2012/03/14. doi: 10.1083/jcb.201112098. PubMed PMID: 22412018; PubMed Central
823 PMCID: PMCPMC3308701.
824 39. Bujalka H, Koenning M, Jackson S, Perreau VM, Pope B, Hay CM, et al. MYRF is a membrane-
825 associated transcription factor that autoproteolytically cleaves to directly activate myelin genes.
826 PLoS biology. 2013;11(8):e1001625. Epub 2013/08/24. doi: 10.1371/journal.pbio.1001625. PubMed
827 PMID: 23966833; PubMed Central PMCID: PMCPMC3742440.
828 40. Emery B, Agalliu D, Cahoy JD, Watkins TA, Dugas JC, Mulinyawe SB, et al. Myelin gene
829 regulatory factor is a critical transcriptional regulator required for CNS myelination. Cell.
830 2009;138(1):172-85. Epub 2009/07/15. doi: 10.1016/j.cell.2009.04.031. PubMed PMID: 19596243;
831 PubMed Central PMCID: PMCPMC2757090.
832 41. Li Z, Park Y, Marcotte EM. A Bacteriophage tailspike domain promotes self-cleavage of a
833 human membrane-bound transcription factor, the myelin regulatory factor MYRF. PLoS biology.
834 2013;11(8):e1001624. Epub 2013/08/24. doi: 10.1371/journal.pbio.1001624. PubMed PMID:
835 23966832; PubMed Central PMCID: PMCPMC3742443.
836 42. Kim D, Choi JO, Fan C, Shearer RS, Sharif M, Busch P, et al. Homo-trimerization is essential
837 for the transcription factor function of Myrf for oligodendrocyte differentiation. Nucleic acids
838 research. 2017;45(9):5112-25. Epub 2017/02/06. doi: 10.1093/nar/gkx080. PubMed PMID:
839 28160598; PubMed Central PMCID: PMCPMC5436001.
840 43. Liao X, Lan C, Liao D, Tian J, Huang X. Exploration and detection of potential regulatory
841 variants in refractive error GWAS. Sci Rep. 2016;6:33090. Epub 2016/09/09. doi: 10.1038/srep33090.
842 PubMed PMID: 27604318; PubMed Central PMCID: PMCPMC5015044.
843 44. Gu SM, Thompson DA, Srikumari CR, Lorenz B, Finckh U, Nicoletti A, et al. Mutations in
844 RPE65 cause autosomal recessive childhood-onset severe retinal dystrophy. Nat Genet.
845 1997;17(2):194-7. Epub 1997/11/05. doi: 10.1038/ng1097-194. PubMed PMID: 9326941.

45. Morimura H, Fishman GA, Grover SA, Fulton AB, Berson EL, Dryja TP. Mutations in the RPE65 gene in patients with autosomal recessive retinitis pigmentosa or leber congenital amaurosis. Proceedings of the National Academy of Sciences of the United States of America. 1998;95(6):3088-93. Epub 1998/04/18. doi: 10.1073/pnas.95.6.3088. PubMed PMID: 9501220; PubMed Central PMCID: PMCPMC19699.

46. Hayward C, Shu X, Cideciyan AV, Lennon A, Barran P, Zareparsi S, et al. Mutation in a short-chain collagen gene, CTRP5, results in extracellular deposit formation in late-onset retinal degeneration: a genetic model for age-related macular degeneration. Human molecular genetics. 2003;12(20):2657-67. Epub 2003/08/29. doi: 10.1093/hmg/ddg289. PubMed PMID: 12944416.

47. Gal A, Rau I, El Matri L, Kreienkamp H-J, Fehr S, Baklouti K, et al. Autosomal-recessive posterior microphthalmos is caused by mutations in PRSS56, a gene encoding a trypsin-like serine protease. The American Journal of Human Genetics. 2011;88(3):382-90.

48. Orr A, Dubé M-P, Zenteno JC, Jiang H, Asselin G, Evans SC, et al. Mutations in a novel serine protease PRSS56 in families with nanophthalmos. Molecular vision. 2011;17:1850.

49. Huang H, Teng P, Du J, Meng J, Hu X, Tang T, et al. Interactive repression of MYRF self-cleavage and activity in oligodendrocyte differentiation by TMEM98 protein. The Journal of neuroscience : the official journal of the Society for Neuroscience. 2018. Epub 2018/09/27. doi: 10.1523/jneurosci.0154-18.2018. PubMed PMID: 30249802.

50. Thaung C, West K, Clark BJ, McKie L, Morgan JE, Arnold K, et al. Novel ENU-induced eye mutations in the mouse: models for human eye disease. Human molecular genetics. 2002;11(7):755-67. Epub 2002/04/04. PubMed PMID: 11929848.

51. White JK, Gerdin A-K, Karp NA, Ryder E, Buljan M, Bussell JN, et al. Genome-wide generation and systematic phenotyping of knockout mice reveals new roles for many genes. Cell. 2013;154(2):452-64.

52. Skarnes WC, Rosen B, West AP, Koutsourakis M, Bushell W, Iyer V, et al. A conditional knockout resource for the genome-wide study of mouse gene function. Nature. 2011;474(7351):337.

53. Wallace HA, Marques-Kranc F, Richardson M, Luna-Crespo F, Sharpe JA, Hughes J, et al. Manipulating the mouse genome to engineer precise functional syntenic replacements with human sequence. Cell. 2007;128(1):197-209. Epub 2007/01/16. doi: 10.1016/j.cell.2006.11.044. PubMed PMID: 17218265.

54. Kleinjan DA, Seawright A, Mella S, Carr CB, Tyas DA, Simpson TI, et al. Long-range downstream enhancers are essential for Pax6 expression. Developmental biology. 2006;299(2):563-81. Epub 2006/10/04. doi: 10.1016/j.ydbio.2006.08.060. PubMed PMID: 17014839; PubMed Central PMCID: PMCPMC2386664.

55. Schindelin J, Arganda-Carreras I, Frise E, Kaynig V, Longair M, Pietzsch T, et al. Fiji: an open-source platform for biological-image analysis. Nature methods. 2012;9(7):676-82. Epub 2012/06/30. doi: 10.1038/nmeth.2019. PubMed PMID: 22743772; PubMed Central PMCID: PMCPMC3855844.

56. Jadeja S, Barnard AR, McKie L, Cross SH, White JK, Robertson M, et al. Mouse slc9a8 mutants exhibit retinal defects due to retinal pigmented epithelium dysfunction. Investigative ophthalmology & visual science. 2015;56(5):3015-26. Epub 2015/03/05. doi: 10.1167/iovs.14-15735. PubMed PMID: 25736793; PubMed Central PMCID: PMCPMC4538965.

57. Kammers K, Cole RN, Tiengwe C, Ruczinski I. Detecting Significant Changes in Protein Abundance. EuPA open proteomics. 2015;7:11-9. Epub 2015/03/31. doi: 10.1016/j.euprot.2015.02.002. PubMed PMID: 25821719; PubMed Central PMCID: PMCPMC4373093.

58. Hornig J, Frob F, Vogl MR, Hermans-Borgmeyer I, Tamm ER, Wegner M. The transcription factors Sox10 and Myrf define an essential regulatory network module in differentiating oligodendrocytes. PLoS Genet. 2013;9(10):e1003907. Epub 2013/11/10. doi: 10.1371/journal.pgen.1003907. PubMed PMID: 24204311; PubMed Central PMCID: PMCPMC3814293.

Table 1. Primary antibodies.

Antibody	Source	Product No	Concentration used
anti-AIF	Cell Signaling Technology	5318	1:5000 (WB)
anti-Ezrin	abcam	ab4069	1:100 (IF)
anti-FLAG	Cell Signaling Technology	2368	1:2000 (WB)
anti-FLAG	BioLegend	637302	1:1000 (IF)
anti-GFAP	abcam	ab7260	1:500 (IF)
anti-GFP	Molecular Probes	A-11122	1:1000 (IF)
anti-MEK1/2	Cell Signaling Technology	8727	1:5000 (WB)
anti-MYC	Cell Signaling Technology	2276	1:2000 (WB)
anti-MYC	Cell Signaling Technology	2278	1:200 (IF)
anti-MYRF (C-terminal)	gift from B. Emery [39]	-	1:500 (IF)
anti-MYRF (N-terminal)	gift from M. Wegner [58]	-	1:500 (IF)
anti-Opsin, red/green	Millipore	AB5405	1:500 (IF)
anti-Rhodopsin	Millipore	MAB5356	1:500 (IF)
anti-TMEM98	proteintech	14731-1-AP	1:5000 (WB), 1:200 (IF)
anti-α-tubulin	Sigma-Aldrich	T5168	1:10,000 (WB)
anti-V5	Invitrogen	46-0705	1:5000 (WB) (IF, Fig 6B), 1:400 (IF, Fig 7)
anti-vimentin	Cell Signaling Technology	5741	1:5000 (WB)
anti-ZO1	Thermo Fisher Scientific	33-9100	1:100 (IF)

Key: WB=Western blotting, IF=immunofluorescence

Figure Legends

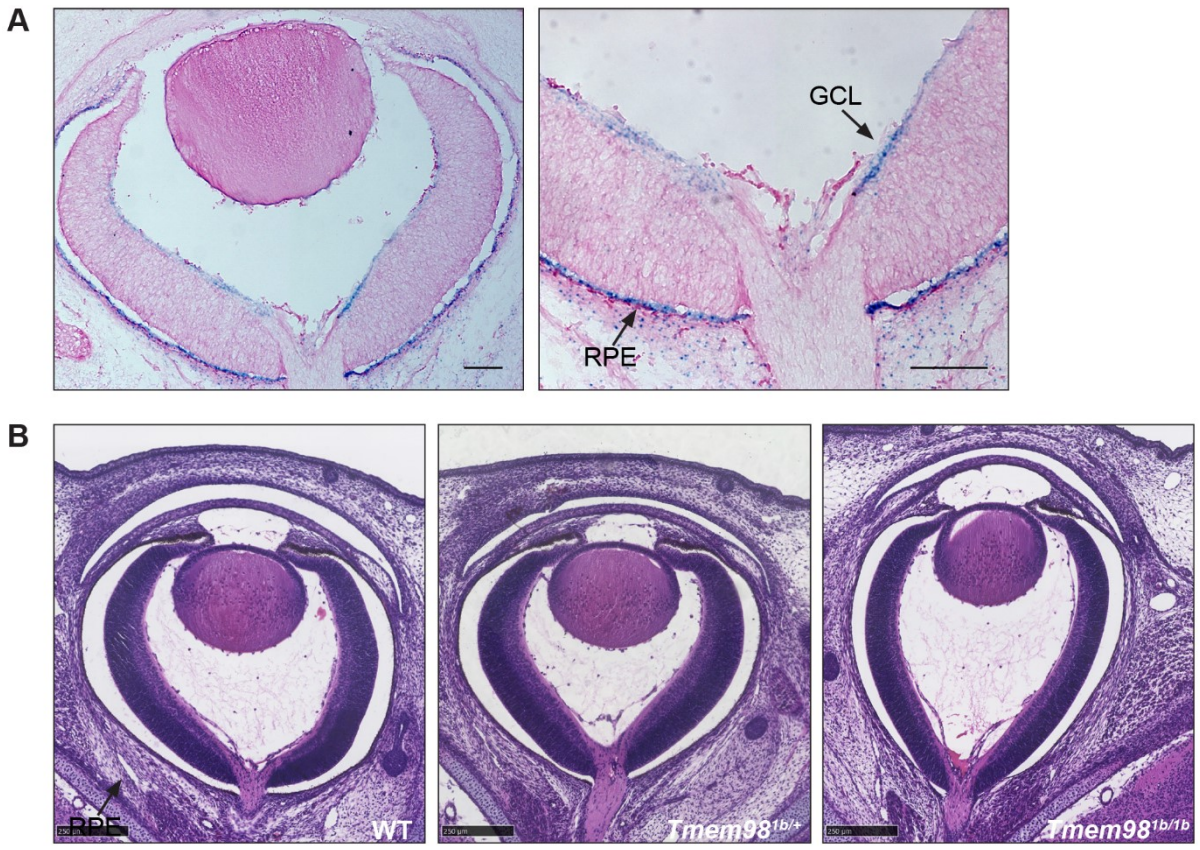

Fig 1. Loss-of function of *Tmem98* results in an elongated eye shape. (A) LacZ stained *Tmem98*$^{tm1b/+}$ E16.5 eye cryosections. The expression pattern of *Tmem98*, indicated by the blue staining for the reporter knockout allele *Tmem98*^{tm1b}, is found predominantly in the RPE and is also observed in the ganglion cell layer. (B) H&E stained eye sections of wild-type (left), *Tmem98*$^{tm1b/+}$ (centre) and *Tmem98*$^{tm1b/tm1b}$ (right) E16.5 littermate embryos. The eye shape is elongated in the *Tmem98* $^{tm1b/tm1b}$ embryo compared to the wild-type and heterozygous embryos. Abbreviations: GCL, ganglion cell layer and RPE, retinal pigment epithelium. Scale bars represent 100 µm (A), 250 µm (B).

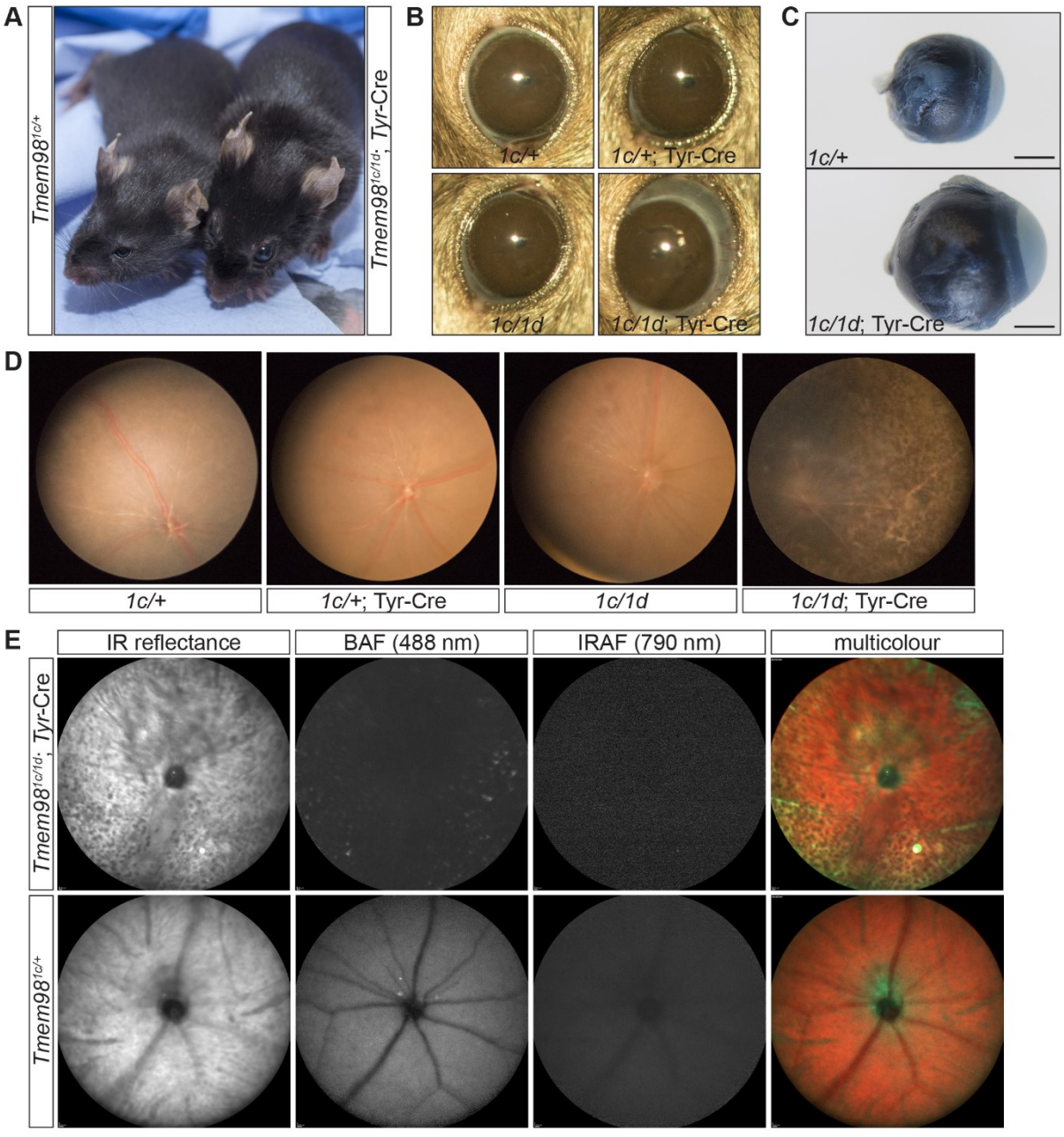

911

912 **Fig 2. Loss-of-function of *Tmem98* in the eye leads to an enlarged eye and**
913 **retinal defects.** (A) *Tmem98*$^{tm1c/+}$ (left) and *Tmem98*$^{tm1c/tm1d}$; Tyr-Cre (right) 9 week
914 old female littermates are shown. When *Tmem98* is knocked-out by Tyr-Cre the eyes
915 are noticeably enlarged. (B) Slit-lamp pictures of 9 week old littermates. The eyes of
916 *Tmem98*$^{tm1c/+}$ (female), *Tmem98*$^{tm1c/+}$; Tyr-Cre (male) and *Tmem98*$^{tm1c/tm1d}$ (female)
917 mice are normal indicating that haploinsufficiency for *Tmem98* and expression of
918 Tyr-Cre does not affect eye size. In contrast the *Tmem98*$^{tm1c/tm1d}$; Tyr-Cre (female)

eye, where *Tmem98* expression is lost, is enlarged and bulges out of the head. (C) Comparison of *Tmem98*$^{tm1c/+}$ (top) and *Tmem98*$^{tm1c/+}$; Tyr-Cre (bottom) enucleated eyes. The eyes were collected from female littermates at three months of age. The posterior segment of the eye is enlarged in the *Tmem98*$^{tm1c/+}$; Tyr-Cre eye. Scale bar represents 1mm. (D) Fundus images of *Tmem98*$^{tm1c/+}$ (female), *Tmem98*$^{tm1c/+}$; Tyr-Cre (male), *Tmem98*$^{tm1c/tm1d}$ (female) and *Tmem98*$^{tm1c/tm1d}$; Tyr-Cre (female) mice. The pictures were taken at 7 weeks of age for the first three and at 10 weeks of age for the fourth. There is extensive retinal degeneration in the *Tmem98*$^{tm1c/tm1d}$; Tyr-Cre whilst the retinas of the other genotypes are normal. (E) Scanning laser ophthalmoscope images of control (*Tmem98*$^{tm1c/+}$) and mutant (*Tmem98*$^{tm1c/tm1d}$; Tyr-Cre) eyes from female littermates at 15 weeks of age. Abbreviations: IR, Infrared; BAF, blue autofluorescence and IRAF, near infrared.

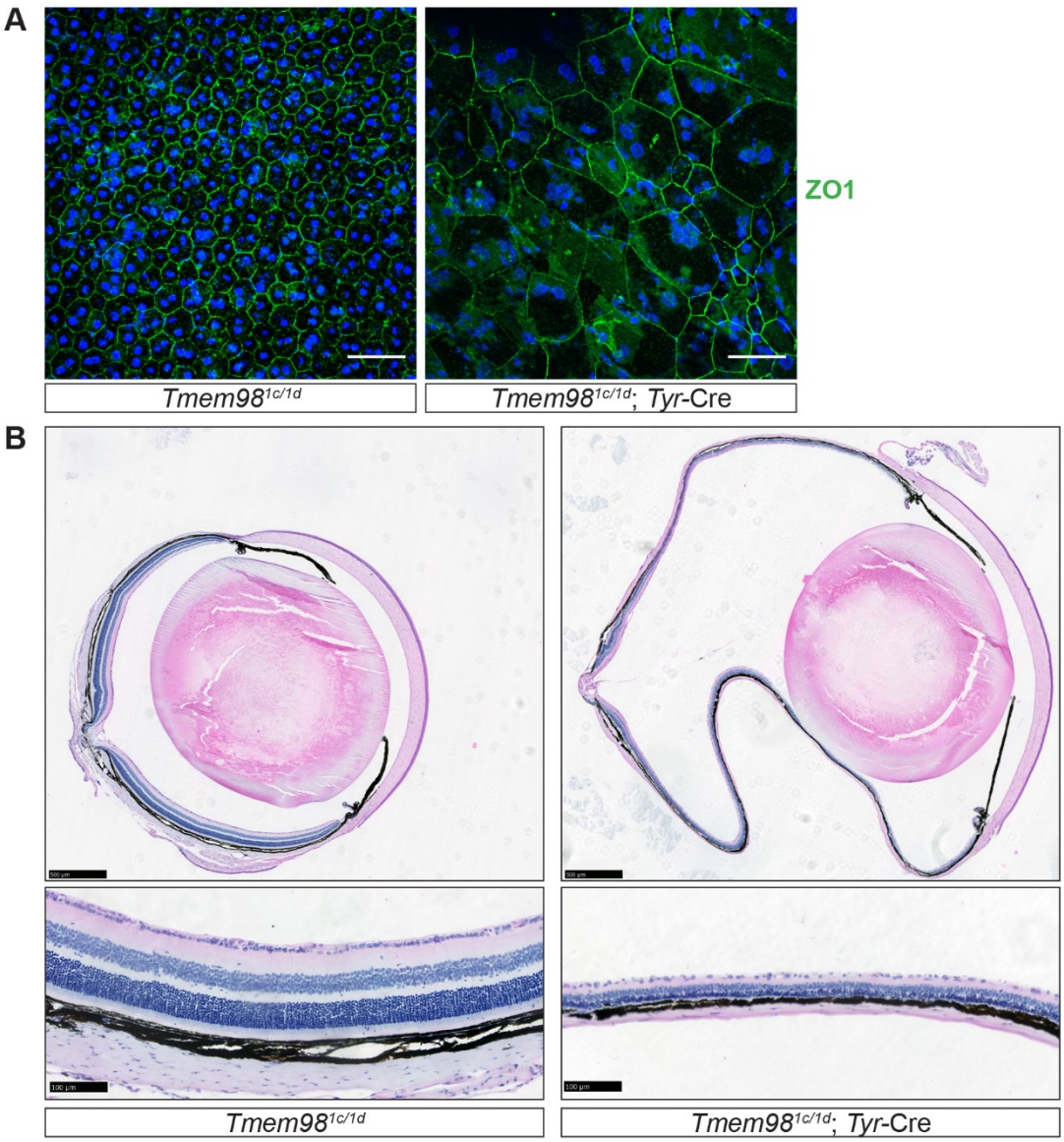

Fig 3. Characterisation of the phenotype caused by loss-of-function of *Tmem98* in the eye. (A) Staining of RPE flat mounts with an anti-ZO1 antibody (green) and DAPI (blue) reveals the regular hexagonal shape of the cells which contain one or two nuclei in the control *Tmem98*$^{tm1c/tm1d}$ RPE. In contrast, the cells in the *Tmem98*$^{tm1c/tm1d}$; Tyr-Cre RPE vary greatly in size, the number of sides they have and many are multinuclear. The RPEs were collected from male littermates at 7 weeks of age. (B) H&E stained adult eye sections. The *Tmem98*$^{tm1c/tm1d}$; Tyr-Cre retina is hugely expanded and very thin compared to the control *Tmem98*$^{tm1c/tm1d}$ retina. In addition, it appears to have lost structural integrity as indicated by the

942 folding of the retina that occurred during processing which is not seen in the control.
943 All the layers of the retina appear to be present (bottom) but are all extremely thin
944 and the choroid is compressed. The eyes were collected from female littermates at
945 16 weeks of age. Scale bars represent 50 μm (A), 500 μm (B, top) and 100 μm (B,
946 bottom).

947

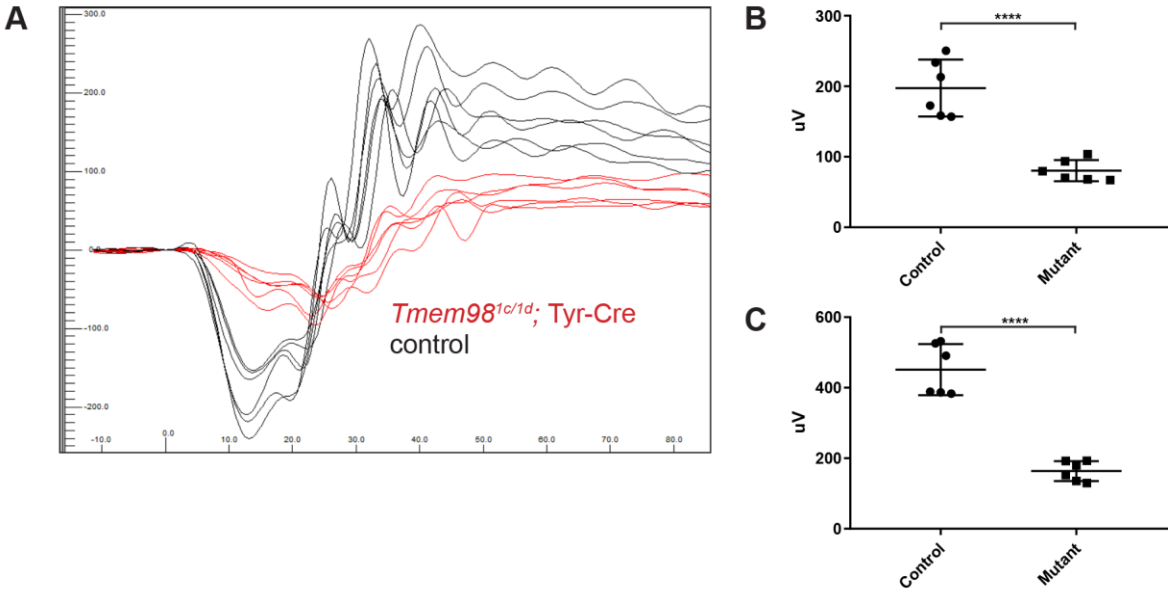

948

949 **Fig 4. Loss-of-function of *Tmem98* in the eye results in an attenuated ERG**
950 **response.** Three *Tmem98*$^{tm1c/tm1d}$; Tyr-Cre female mice and three control female
951 mice (two *Tmem98*$^{tm1c/tm1d}$ and one *Tmem98*$^{tm1c/+}$; Tyr-Cre) were tested at six months
952 of age. (A) ERG traces of *Tmem98*$^{tm1c/tm1d}$; Tyr-Cre mice (red lines) and control mice
953 (black lines). Shown are the responses at 3 cd.s/m^2 (average of four flashes) for all
954 eyes. (B) Comparison of a-wave amplitudes between the mutant *Tmem98*$^{tm1c/tm1d}$;
955 Tyr-Cre mice and control mice. There is a significant difference between mutant and
956 control mice (unpaired *t*-test, P < 0.0001). (C) Comparison of b-wave amplitudes
957 between the mutant *Tmem98*$^{tm1c/tm1d}$; Tyr-Cre mice and control mice. There is a
958 significant difference between mutant and control mice (unpaired *t*-test, P < 0.0001).

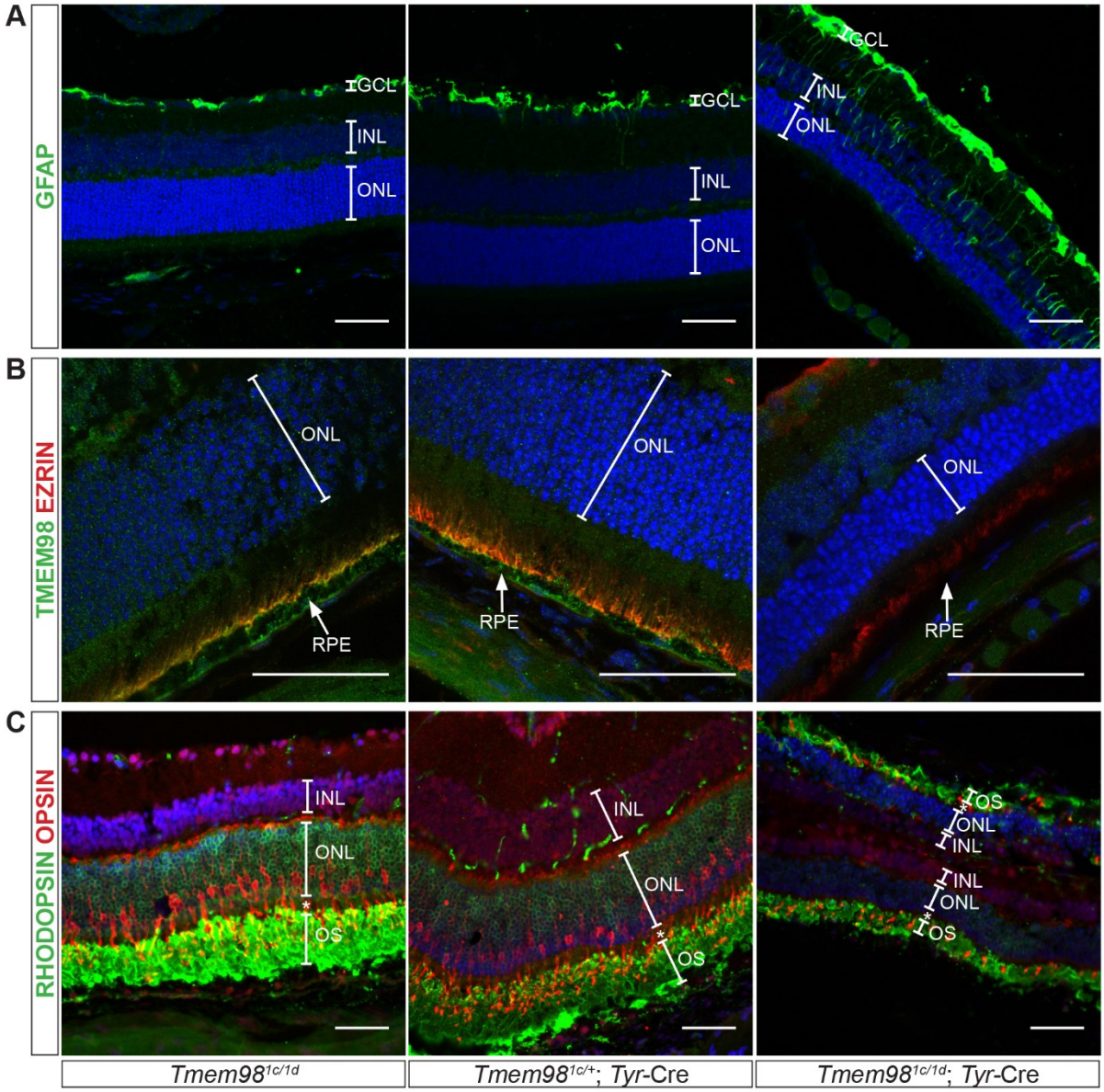

Fig 5. Characterisation of the retinal phenotype caused by loss-of-function of *Tmem98*. Immunostaining of adult retinal sections from control mice (*Tmem98*$^{tm1c/tm1d}$ (left) and *Tmem98*$^{tm1c/+}$; Tyr-Cre (centre)) and mutant mice (*Tmem98*$^{tm1c/tm1d}$; Tyr-Cre (right)). (A) Staining with an anti-GFAP antibody (green) shows that GFAP localisation is normal and seen only in the ganglion cell layer in the control retinas but extends down towards the inner nuclear layer in the mutant retina indicating retinal stress. (B) Staining with anti-TMEM98 (green) and anti-EZRIN (red) antibodies. In the control retinas TMEM98 staining is seen in the apical and basal

968 layers of the RPE and EZRIN is localised to the apical microvilli, co-localisation of
969 the two proteins is indicated by yellow staining. In the mutant retina TMEM98
970 staining is absent and EZRIN appears to be mislocalised. (C) Staining with anti-
971 RHODOPSIN (green) and anti-OPSIN (red) antibodies marking rods and cones
972 respectively. Normal staining is observed in the control retinas but in the mutant
973 although RHODOPSIN and OPSIN are present the outer segment layer is very thin.
974 In the mutant the retina has folded back completely on itself. This is a processing
975 artefact and reflects the fragility of the mutant retina. DAPI staining of DNA is in blue.
976 Abbreviations: inner nuclear layer (INL), outer nuclear layer (ONL), outer segments
977 (OS) and retinal pigment epithelium (RPE). A white asterisk denotes the inner
978 segments. The retinas shown in (A) and (B) were collected from P21 littermate male
979 mice. The retinas shown in (C) were collected from 9 week old littermate male mice.
980 Scale bars represent 50 μm.

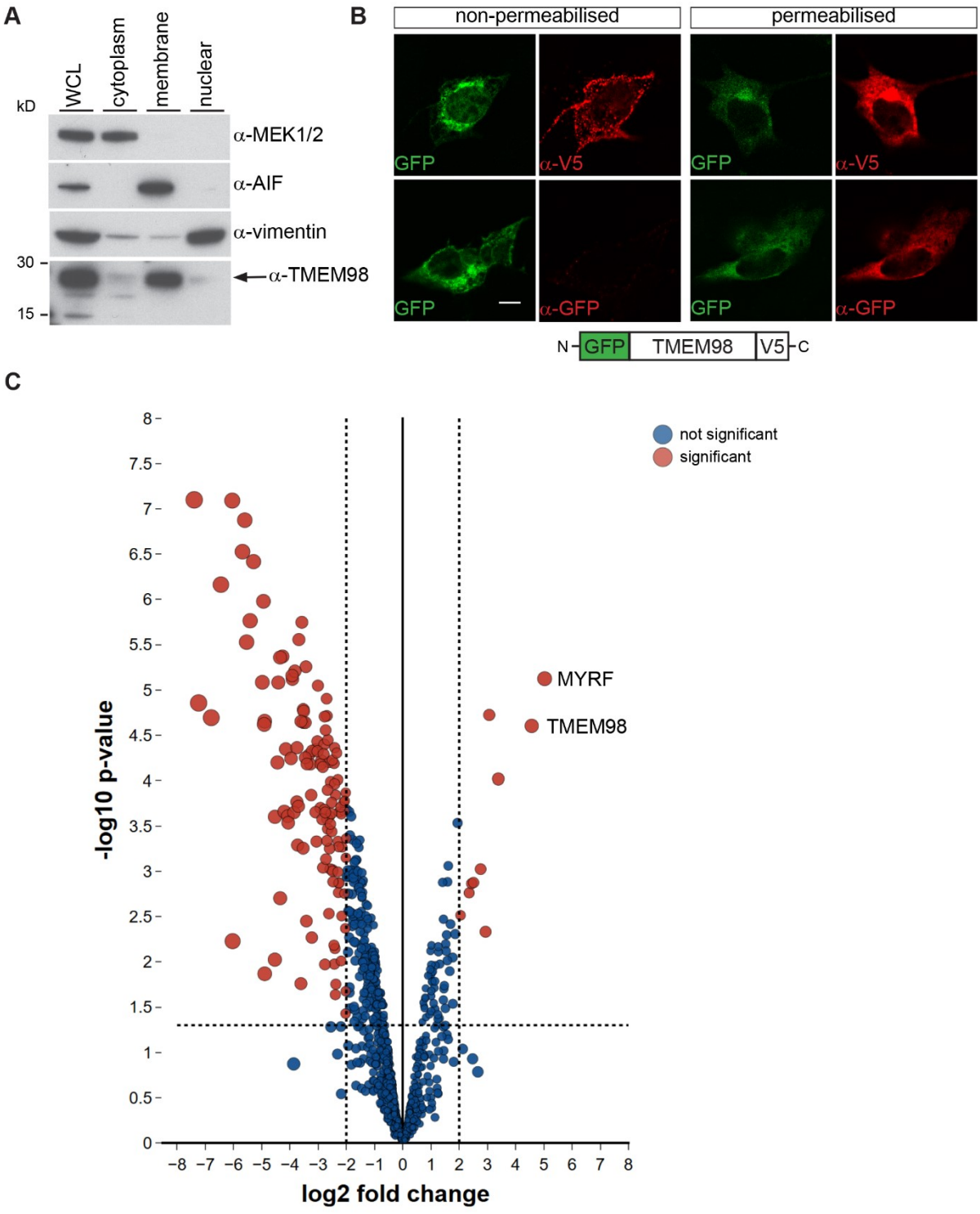

981

982 **Fig 6. TMEM98 is a type II transmembrane protein and interacts with MYRF.** (A)
983 Western blot analysis of ARPE-19 subcellular fractions probed with the indicated
984 antibodies. The control antibodies against MEK1/2, AIF and VIMENTIN are found in
985 the expected fractions. TMEM98 is present in the membrane fraction. WCL= whole

cell lysate (B) Topology of TMEM98. NIH/3T3 cells were transiently transfected with GFP-TMEM98-V5 (green) and immunostained with anti-GFP or anti-V5 antibodies (red). Accessibility to the antibodies indicates that the GFP epitope is intracellular and that the V5 epitope is extracellular. A schematic of the expression GFP-TMEM98-V5 construct is shown below. (C) Volcano plot of the mass spectrometry data comparing proteins biotinylated by TMEM98-BirA* with those by BirA* alone. The x axis is log2 fold change of TMEM98-BirA* peptides versus BirA* peptides and the y axis is –log10 p-value of significance. The horizontal dashed line shows where $p = 0.05$ ($-\log10(0.05) = 1.3$) and the vertical dashed lines show where fold change is four. Proteins with significant difference and change greater than four-fold are shown in red, other proteins are shown in blue. The two most highly enriched proteins, TMEM98 and MYRF, are labelled.

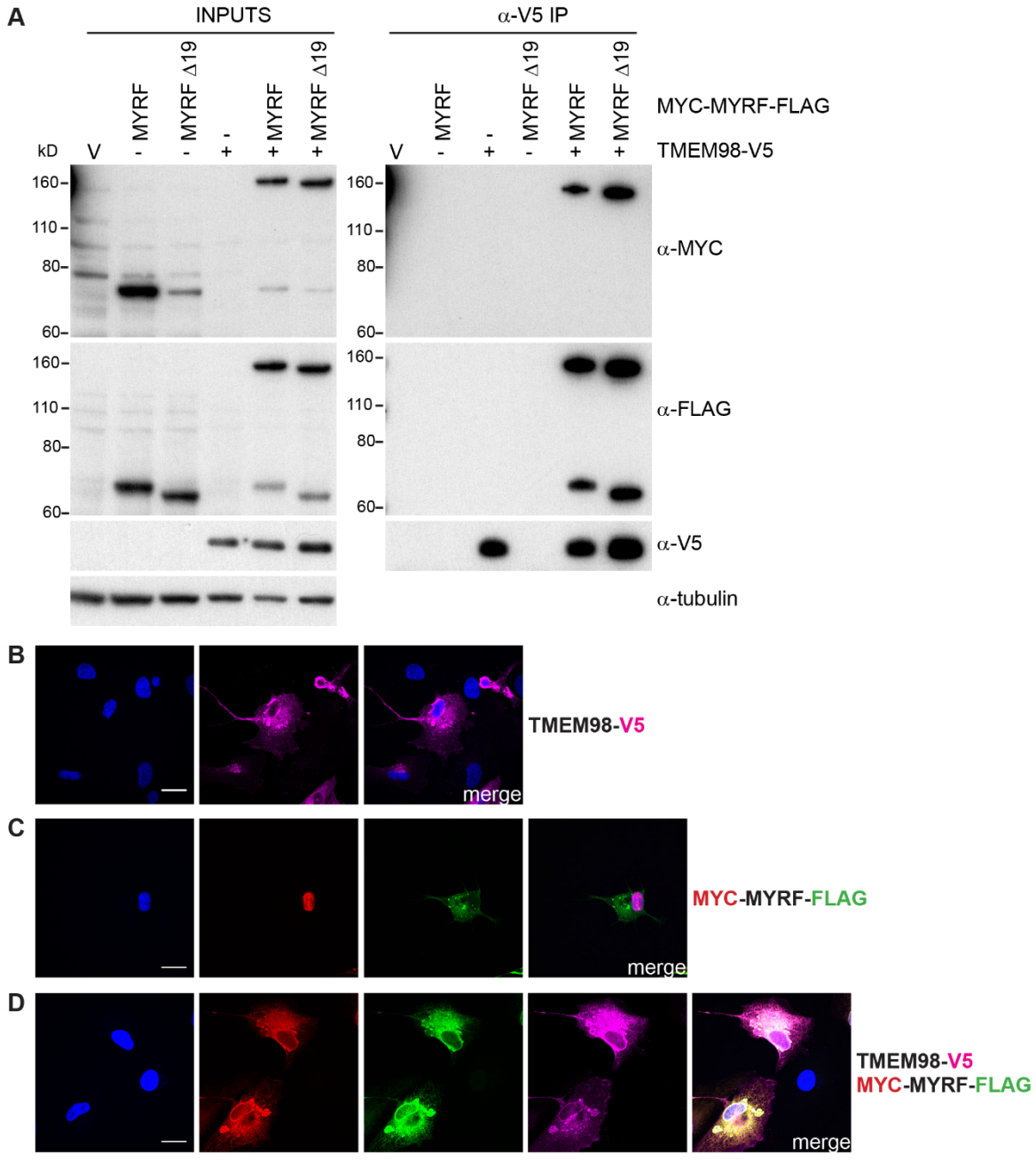

Fig 7. TMEM98 prevents MYRF self-cleavage and binds to the C-terminal part of MYRF. (A) Co-immunoprecipitation experiment where HEK293T cells were transiently transfected with the indicated epitope-tagged expression constructs and immunoprecipitated with anti-V5.The two MYRF constructs were either full-length (MYRF) or lacked exon 19 (MYRF Δ19). Western blot analysis of the inputs (left) and immunoprecipitated fractions (right) probed with anti-MYC (Cell Signaling Technology, 2276), anti-FLAG (Cell Signaling Technology, 2368) and anti-V5

antibodies are shown. Anti-tubulin antibody was used to probe the input Western as a loading control. The Western of the input samples shows that MYRF cleaves when transfected alone but remains largely intact when co-transfected with TMEM98-V5. The Western of the immunoprecipitated fractions shows that intact MYC-MYRF-FLAG and the C-terminal part tagged with FLAG are co-immunoprecipitated with TMEM98-V5 indicating that TMEM98 interacts with the C-terminal part of MYRF. (B-D) ARPE-19 cells were transiently transfected with TMEM98-V5 and/or MYC-MYRF-FLAG and immunostained with anti-V5 (magenta), anti-MYC (Cell Signaling Technology, 2278) (red) and anti-FLAG (Biolegend, 637302) (green) antibodies as indicated. DAPI staining is in blue. (C) When transfected alone MYC-MYRF-FLAG cleaves and the N-terminal part tagged with MYC translocates to the nucleus whilst the C-terminal part tagged with FLAG is membrane-bound. (D) When MYC-MYRF-FLAG is co-transfected with TMEM98-V5 it remains intact and colocalises with TMEM98-V5 in the membrane. Scale bars represent 20 μm.

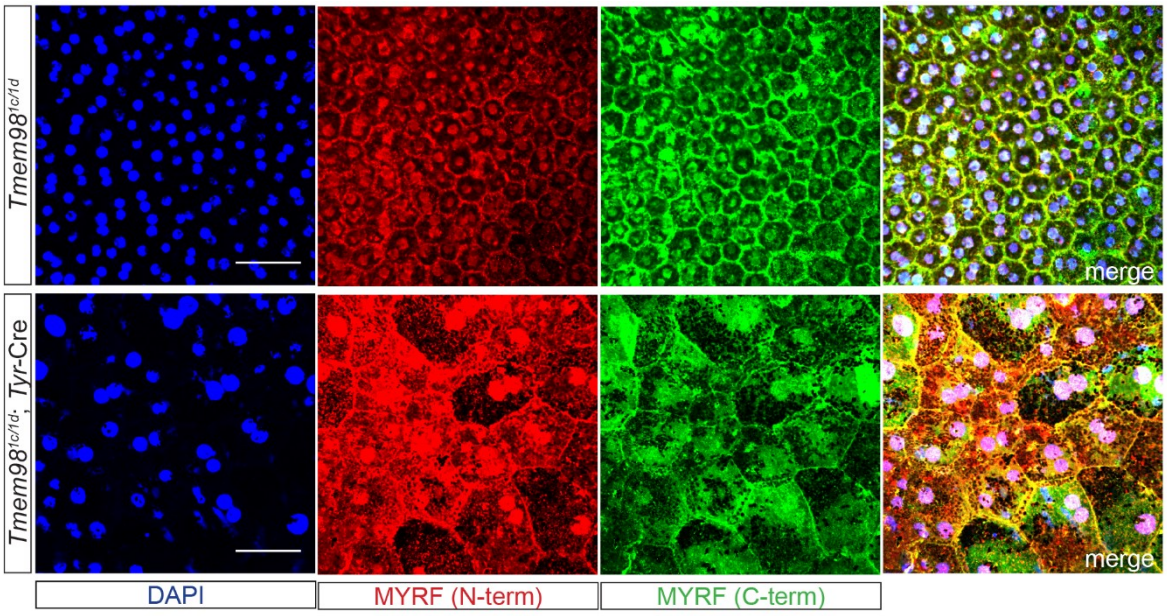

Fig 8. MYRF is mislocalised in the RPE when *Tmem98* is knocked-out in the eye. Immunostaining of control *Tmem98*$^{tm1c/tm1d}$ (top) and mutant *Tmem98*$^{tm1c/tm1d}$; Tyr-Cre RPE flat mounts with DAPI (blue), anti-MYRF N-terminal (red) and anti-MYRF C-terminal (green) antibodies. MYRF staining is aberrant and when compared to the control more of N-terminal part of MYRF appear to be present in the nucleus in the mutant when compared to the control. The RPEs were collected from P26 male littermate mice. Scale bars represent 50 μm.

Supporting Information

S1 Table. Genotyping primers.

Primer Name	Sequence (5'-3')	Product size (allele)
1532	CCAAAGGGGTGCATTTGAAG	465 bp (WT)
1533	TGCAAACCCAAGTCAAAAAGC	595 bp (*tm1c*)
1532	CCAAAGGGGTGCATTTGAAG	196 bp (*tm1a*, *tm1b*, *tm1c*, *tm1d*)
1490	TCGTGGTATCGTTATGCGCC	
1604	CCCCCTGAACCTGAAACATA	310 bp (*tm1b*)
838	CTCAGACACCCAGCCTTCTC	
1605	ACCCTTCTCTCCCTAAGTAGTCT	867 bp (WT)
1606	CCCCAAGCCGTCCTTTCC	1030 bp (*tm1c*)
		238 bp (*tm1d*)
FLPeF	AGGGTGAAAGCATCTGGGAGA	~400 bp (FLPe)
FLPeR	TCAACTCCGTTAGGCCCTTCA	
747	CCTGGAAAATGCTTCTGTCCG	4 primer reaction
748	CAGGGTGTTATAAGCAATCCC	290 bp (control product)
749	AACACACACTGGAGGACTGGCTA	450 bp (Cre)
750	CAATGGTAGGCTCACTCTGGGAG	

Supporting Information Captions

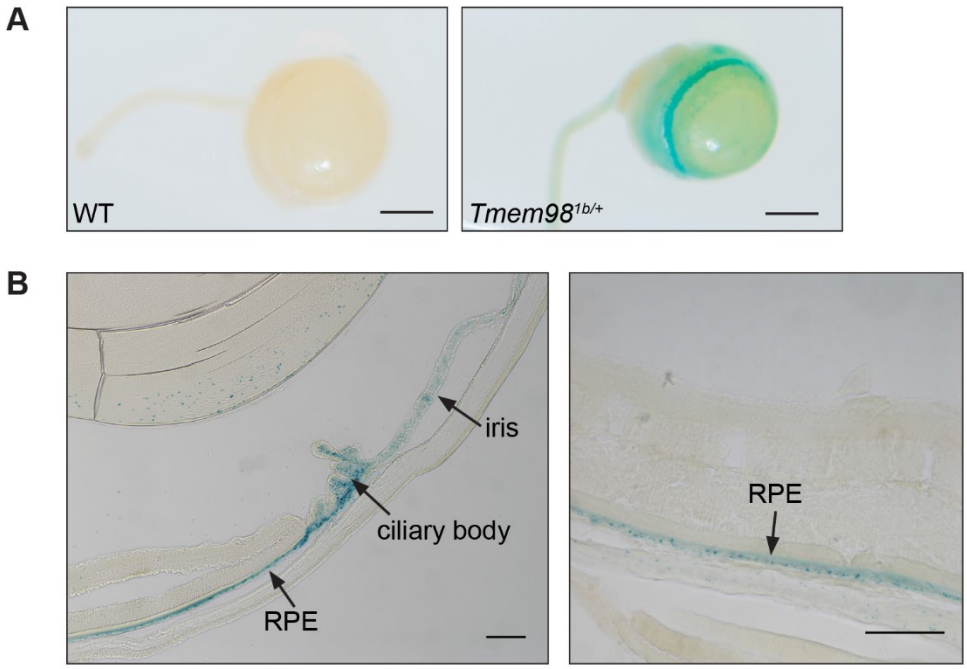

S1 Fig. *Tmem98* is expressed in the adult RPE, ciliary body and iris. (A) LacZ staining of wild-type (male) and *Tmem98*$^{tm1b/+}$ (female) adult albino eyes collected at 5 weeks. The expression pattern of *Tmem98* is indicated by the blue staining for the reporter knockout allele *Tmem98*^{tm1b}. Eyes were enucleated and fixed in 4% PFA/PBS for an hour, rinsed in PBS and washed three times in detergent buffer (0.1 M phosphate buffer pH7.3, 2 mM $MgCl_2$, 0.1% sodium deoxycholate and 0.02% NP-40 (IGEPAL CA-630)). The eyes were then stained in detergent buffer containing 14.5 mM NaCl, 5 mM $K_3Fe(CN)_6$, 5 mM $K_4[Fe(CN)_6].3H_20$ and 150 µg X-gal (5-bromo-4-chloro-3-indolyl-β-D-galactopyranoside) at 37°C protected from light, washed twice in detergent buffer, post-fixed overnight in 4% PFA/PBS, rinsed in PBS and photographed. (B) Cryosections of LacZ-stained *Tmem98*$^{tm1b/+}$ (male) adult albino eye collected at 6 weeks show that *Tmem98* is strongly expressed in the RPE, ciliary body and iris. Cryosections were prepared as described in Materials and Methods and coverslips mounted in Vectashield (Vector Laboratories) prior to brightfield imaging. Scale bars represent 1 mm (A) and 100 µm (B).

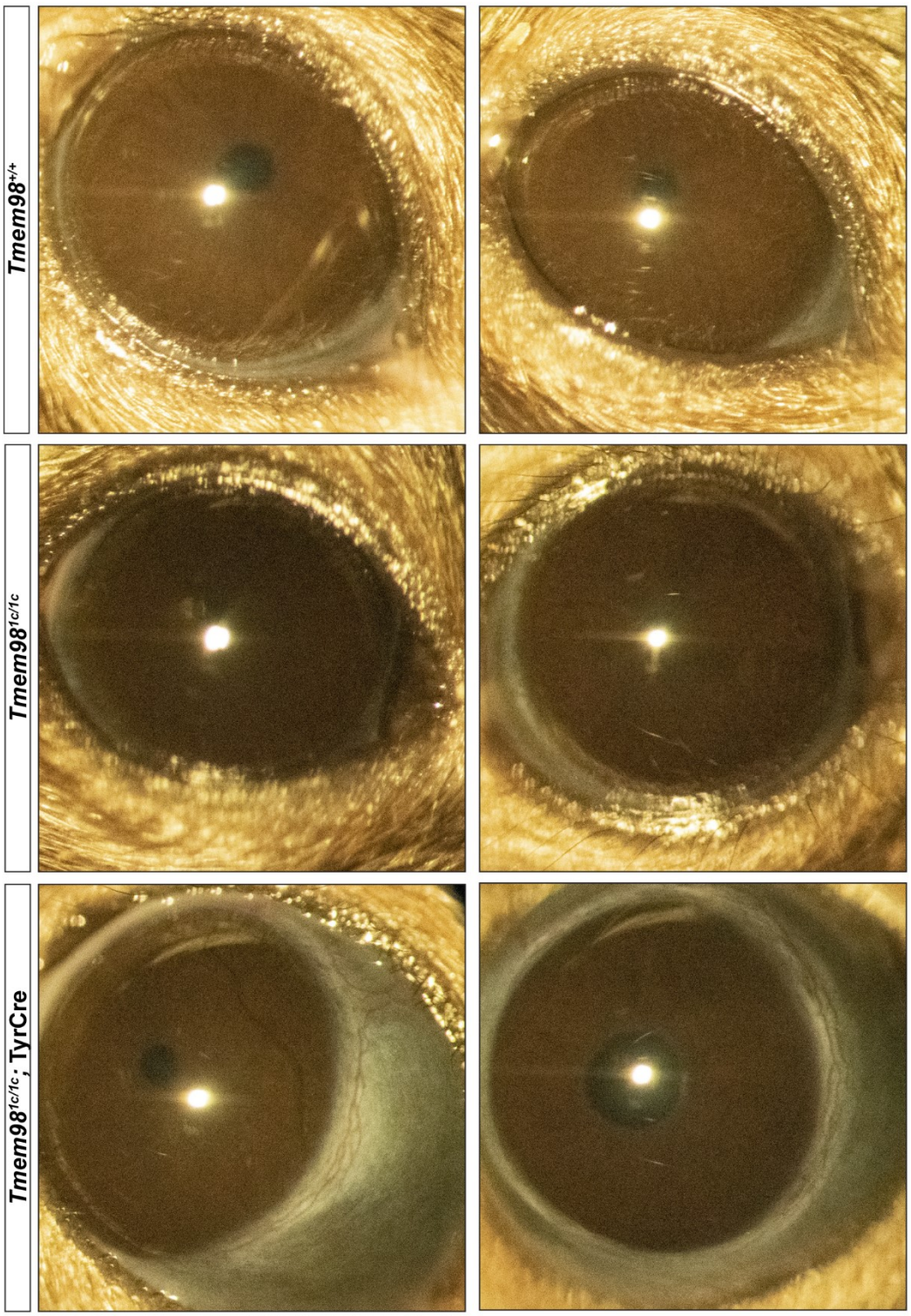

S2 Fig. *Tmem98*$^{tm1c/tm1c}$ mice have normal eyes. Shown are slit-lamp pictures of eyes from two wild-type mice (top row), two *Tmem98*$^{tm1c/tm1c}$ mice (middle row) and two *Tmem98*$^{tm1c/tm1c}$; Tyr-Cre mice (bottom row). The mice in the top row are a female on the left and a male on the right at 11 weeks of age. The mice in the middle

and bottom rows are female 9 week old littermates. Mice homozygous for the floxed conditional allele *Tmem98*^{tm1c} have eyes of normal size, whereas the eyes of the *Tmem98*$^{tm1c/tm1c}$; Tyr-Cre mice are enlarged.

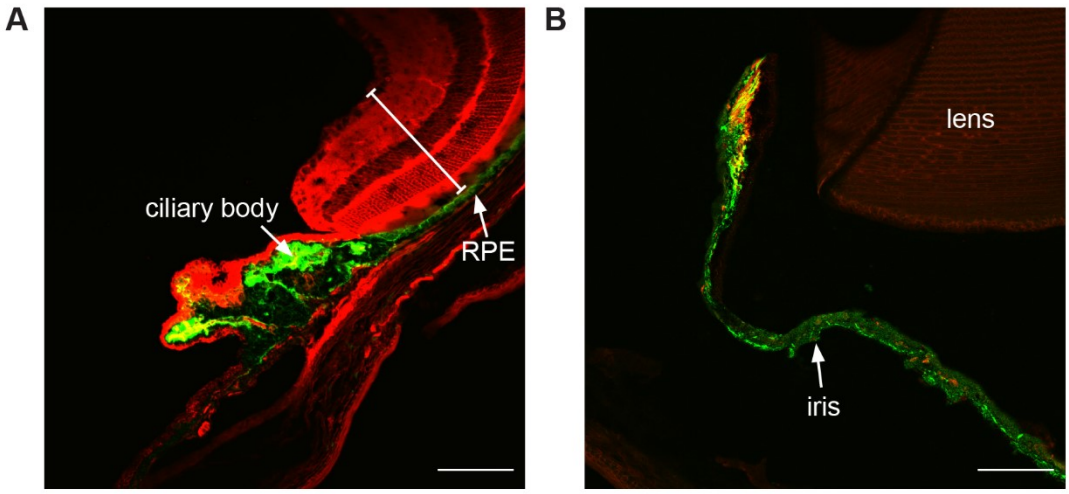

S3 Fig. Tyr-Cre is expressed in the RPE, ciliary body and RPE. Cryosections of adult R26MTMG; Tyr-Cre eye showing that Cre is expressed in the RPE, ciliary body and iris and in the neural retina (denoted by a white bar), lens or elsewhere in the eye. Tomato fluorescent protein (red) and green fluorescent protein (green). Scale bars represent 100 μm.

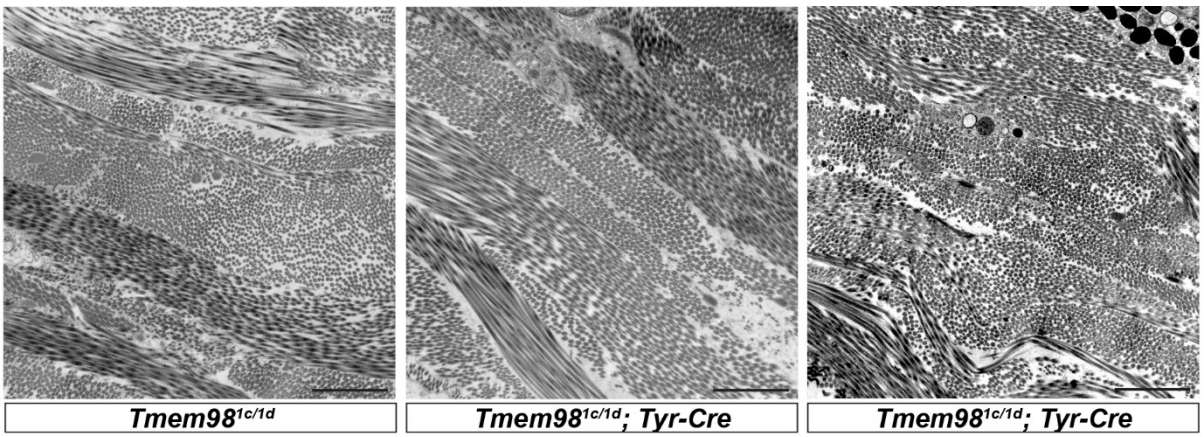

S4 Fig. Ultrastructural analysis of the sclera. Eyes from four month old male littermate mice were fixed overnight in 3% glutaraldehyde in cacodylate buffer at 4°C then post-fixed in 1% osmium tetroxide for two hours at 4°C. After dehydration through ascending grades of alcohol and propylene oxide they were impregnated with TAAB Embedding Resin (medium grade premix) and cured for 24 hours. Ultrathin sections were stained with uranyl acetate and lead citrate and viewed on a JEOL JEM 1200 EX2 transmission electron microscope fitted with an AMT Digital Camera using the AMTv600 image capture software. There does not appear to be any difference in the collagen bundle structure between the control *Tmem98*$^{tm1c/1d}$ (left) and mutant *Tmem98*$^{tm1c/tm1d}$; Tyr-Cre (centre and right). Scale bars represent 2 µm.

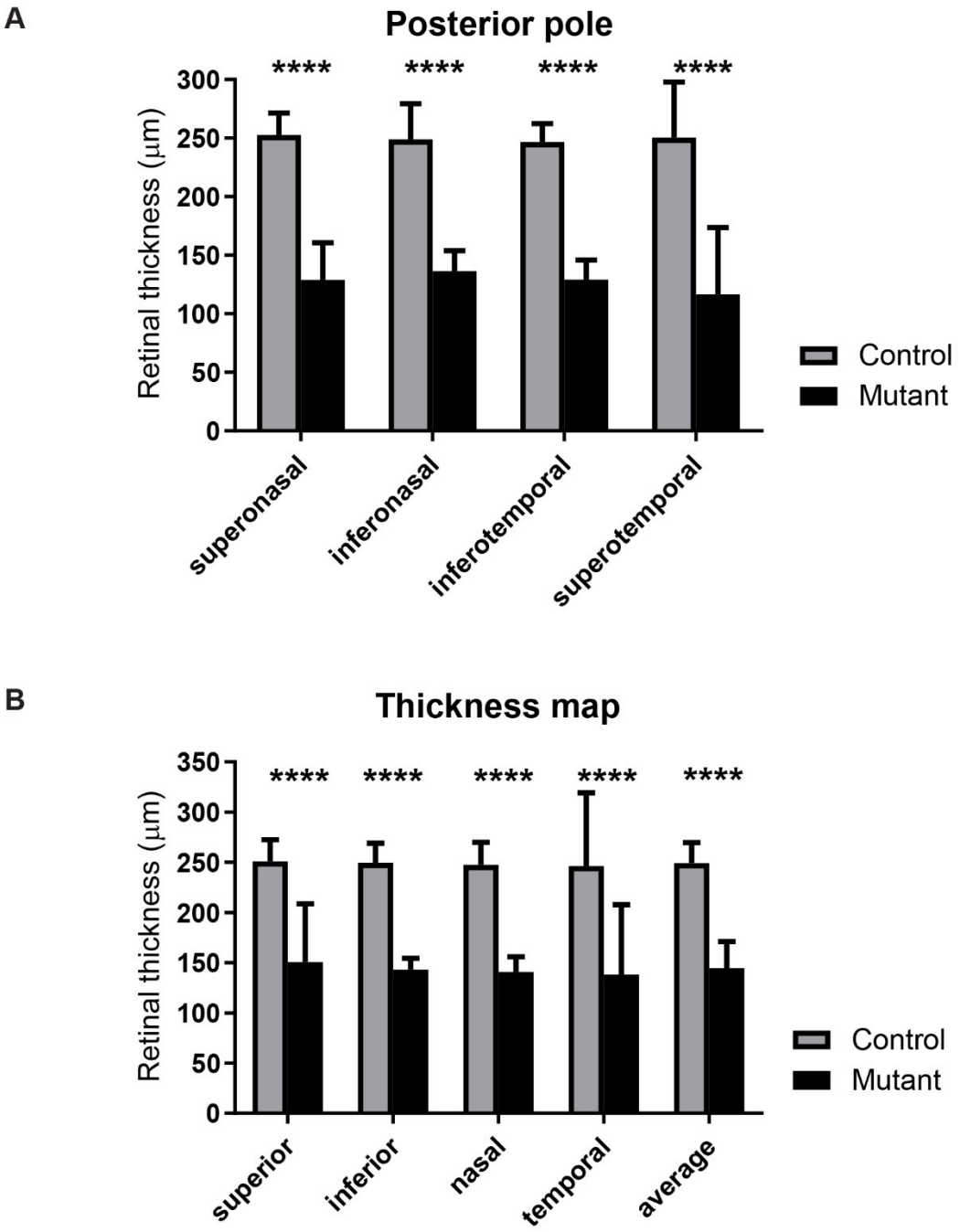

1079

1080 **S5 Fig. Posterior pole and ETDRS grid retinal thickness measurements.** Shown
1081 is the data from three control *Tmem98*$^{tm1c/+}$ mice (one male and two females) and
1082 three female mutant *Tmem98*$^{tm1c/tm1d}$; Tyr-Cre mice aged between 10 and 14 weeks.
1083 (A) Posterior pole retinal thickness measurements. (B) Early Treatment Diabetic
1084 Retinopathy Study (ETDRS) grid thickness map. In both cases the retinal thickness
1085 is significantly decreased in the mutant. Key: **** = P < 0.0001 (Two-way ANOVA).

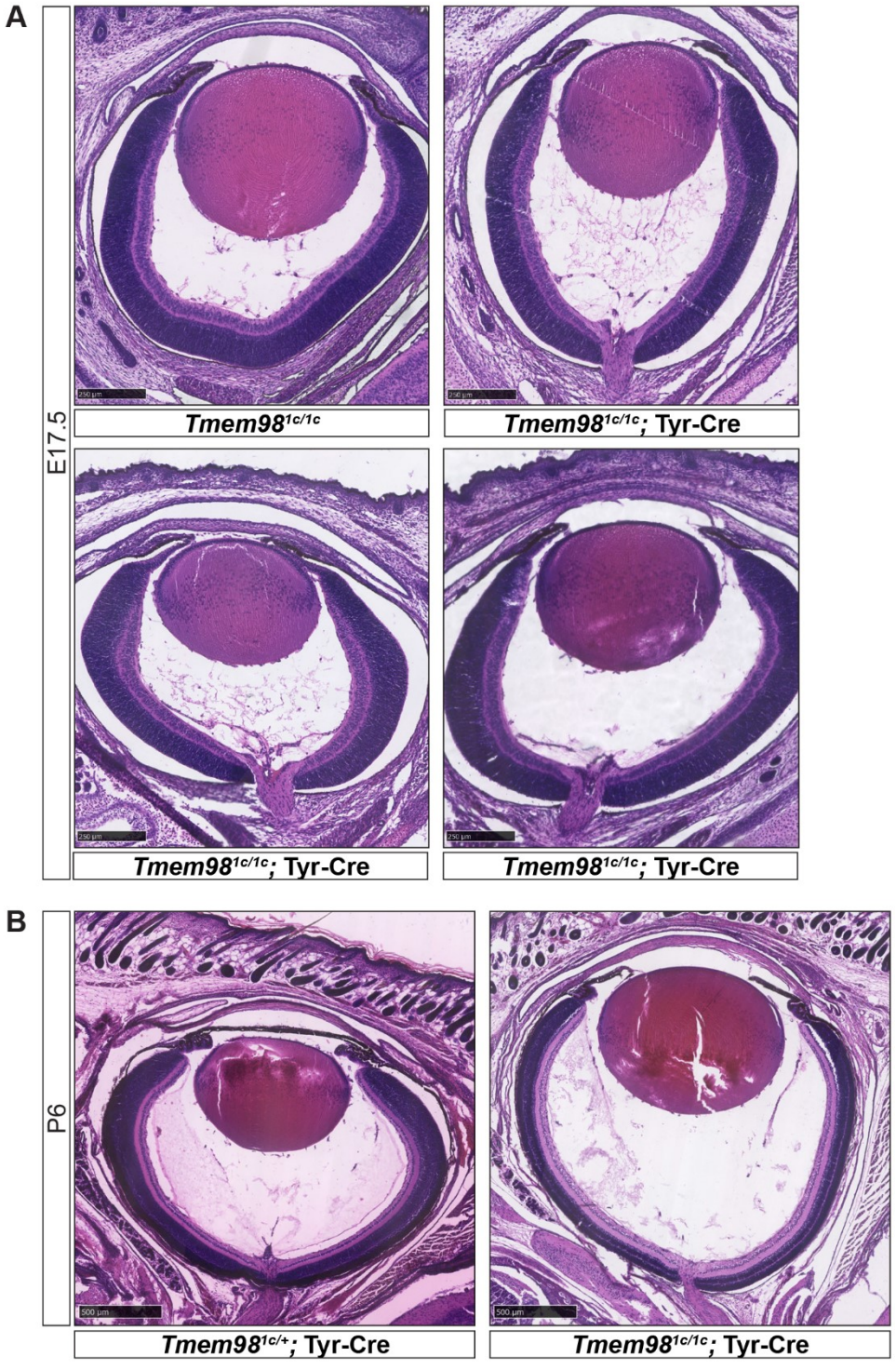

S6 Fig. Eye shape is elongated when *Tmem98* is knocked-out in the eye by P6. H&E stained head sections are shown. (A) Sections through the eye for one control *Tmem98*$^{tm1c/tm1c}$ and three mutant *Tmem98*$^{tm1c/tm1c}$; Tyr-Cre E17.5 embryos. The eye shape is noticeably elongated in one of the *Tmem98*$^{tm1c/tm1c}$; Tyr-Cre embryos (top

right) compared to the control (top left). (B) Sections through the eye for control *Tmem98*$^{tm1c/+}$; Tyr-Cre (left) and mutant *Tmem98*$^{tm1c/tm1c}$; Tyr-Cre P6 mice. The posterior segment of the mutant *Tmem98*$^{tm1c/tm1c}$; Tyr-Cre eye is expanded and the retinal layers are thinner compared to the control. For P6 samples mice were culled and following decapitation and removal of the lower jaw heads were fixed in Davidson's fixative at 4°C. Otherwise they were processed as described for embryos in Materials and Methods except that they were sectioned at 16 μm. Scale bars represent 250 μm (A) and 500 μm (B).

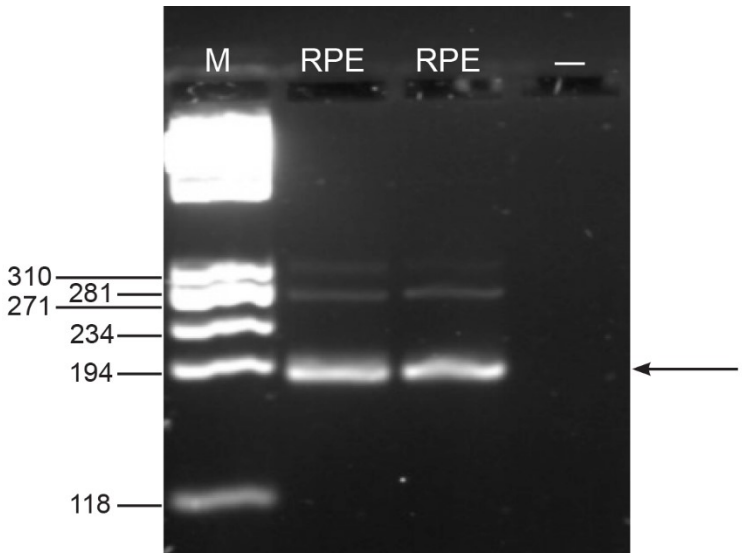

S7 Fig. The predominant RPE *Myrf* transcript splice form lacks exon 19. Shown is RT-PCR analysis of RPE collected from two C57BL/6 mice. The forward primer used was from exon 17 (5'-TAGCTCTGGTGGTGGTCATG-3') and the reverse primer spanned the exon 20/21 boundary (5'-GTAACCAGCAGCAAAGAGGG-3'). The predicted RT-PCR product sizes are 268 bp if exon 19 is included and 187 bp if exon 19 is excluded. The predominant splice form present in RPE is 187 bp (arrowed) which lacks exon 19. This was confirmed by sequencing. The sizes of the DNA fragments in the marker lane (M) are indicated to the left. The lane labelled with

dash is a no template control. RNA was prepared using an RNeasy Plus Micro kit (Qiagen) following the manufacturer's instructions and first strand cDNA was prepared using a GoScript Reverse Transcription System (Promega).

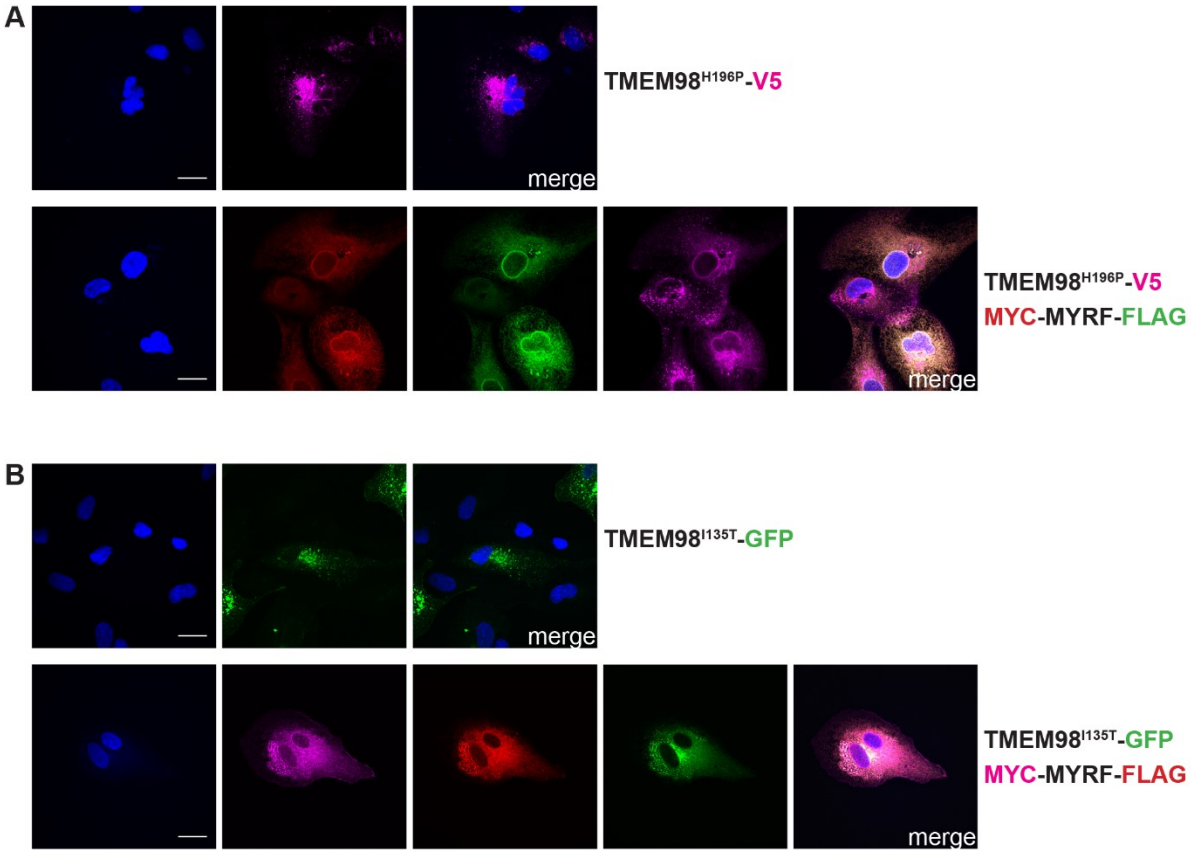

S8 Fig. Mutations H196P and I135T of TMEM98 do not affect its ability to inhibit MYRF self-cleavage. (A) ARPE-19 cells were transiently transfected with TMEM98^{H196P}-V5 alone (top) or with MYC-MYRF-FLAG (bottom) and immunostained with anti-V5 (magenta), anti-MYC (Cell Signaling Technology, 2278) (red) and anti-FLAG (Biolegend, 637302) (green) antibodies as indicated. DAPI staining is in blue. When MYC-MYRF-FLAG is co-transfected with TMEM98^{H196P}-V5 it remains intact and colocalises with TMEM98-V5 in the membrane. The TMEM98^{H196P}-V5 construct was made in the same way as the TMEM98-V5 construct except that *Tmem98* open

reading frame with the initiating ATG was amplified from cDNA isolated from *Tmem98*$^{H196P/H196P}$ mice. (B) ARPE-19 cells were transiently transfected with TMEM98^{I135T}-GFP alone (top) or with MYC-MYRF-FLAG (bottom) and immunostained with anti-MYC (Cell Signaling Technology, 2276) (magenta) and anti-FLAG (Cell Signaling Technology, 2368) (green) antibodies as indicated. TMEM98^{I135T}-GFP is in green and DAPI staining is in blue. When MYC-MYRF-FLAG is co-transfected with TMEM98^{I135T}-GFP it remains intact and colocalises with TMEM98^{I135T}-GFP in the membrane. To make the TMEM98^{I135T}-GFP construct the *Tmem98* open reading frame with the I135T missense mutation was amplified by PCR using the primers 5'- GGGAGATCTCCCGGCATGCCCTGCTGCTGG-3' and 5'-CCCACCGGTATGGCCGACTGTTCCTGCAG -3' and cloned into the BglII and AgeI sites of pEGFP-N1 (BD Biosciences Clontech). Scale bars represent 20 μm.